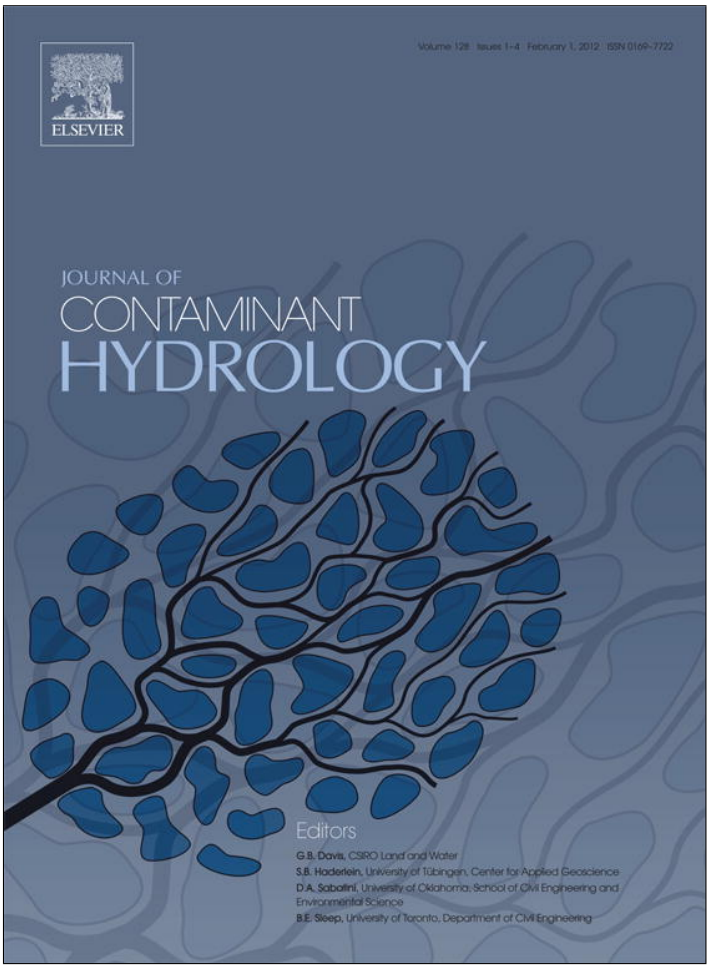

Journal of Contaminant Hydrology 151 (2013) 34–54

Contents lists available at SciVerse ScienceDirect

Journal of Contaminant Hydrology

journal homepage: www.elsevier.com/locate/jconhyd

Identifying key controls on the behavior of an acidic-U(VI) plume in the Savannah River Site using reactive transport modeling

Sergio A. Bea [a,*], Haruko Wainwright [a,1], Nicolas Spycher [a,2], Boris Faybishenko [a,3], Susan S. Hubbard [a,4], Miles E. Denham [b,5]

[a] Earth Sciences Division, Lawrence Berkeley National Lab., 1 Cyclotron Road Mail Stop 90R1116, Berkeley, CA 94720-8126, United States
[b] Savannah River National Lab., Bldg. 773-42A, Aiken, SC 29808, United States

ARTICLE INFO

Article history:
Received 6 August 2012
Received in revised form 12 April 2013
Accepted 18 April 2013
Available online 1 May 2013

Keywords:
Reactive transport modeling
Acidic plume
Vadose zone
Richards equation
Uranium
Surface complexation modeling
Reactive facies
Uncertainty quantification
ASCEM

ABSTRACT

Acidic low-level waste radioactive waste solutions were discharged to three unlined seepage basins at the F-Area of the Department of Energy (DOE) Savannah River Site (SRS), South Carolina, USA, from 1955 through 1989. Despite many years of active remediation, the groundwater remains acidic and contaminated with significant levels of U(VI) and other radionuclides. Monitored Natural Attenuation (MNA) is a desired closure strategy for the site, based on the premise that regional flow of clean background groundwater will eventually neutralize the groundwater acidity, immobilizing U(VI) through adsorption. An in situ treatment system is currently in place to accelerate this in the downgradient portion of the plume and similar measures could be taken upgradient if necessary. Understanding the long-term pH and U(VI) adsorption behavior at the site is critical to assess feasibility of MNA along with the in-situ remediation treatments. This paper presents a reactive transport (RT) model and uncertainty quantification (UQ) analyses to explore key controls on the U(VI)-plume evolution and long-term mobility at this site. Two-dimensional numerical RT simulations are run including the saturated and unsaturated (vadose) zones, U(VI) and H^+ adsorption (surface complexation) onto sediments, dissolution and precipitation of Al and Fe minerals, and key hydrodynamic processes are considered. UQ techniques are applied using a new open-source tool that is part of the developing ASCEM reactive transport modeling and analysis framework to: (1) identify the complex physical and geochemical processes that control the U(VI) plume migration in the pH range where the plume is highly mobile, (2) evaluate those physical and geochemical parameters that are most controlling, and (3) predict the future plume evolution constrained by historical, chemical and hydrological data. The RT simulation results show a good agreement with the observed historical pH and concentrations of U(VI), nitrates and Al concentrations at multiple locations. Mineral dissolution and precipitation combined with adsorption reactions on goethite and kaolinite (the main minerals present with quartz) could buffer pH at the site for long periods of time. UQ analysis using the Morris one-at-a-time (OAT) method indicates that the model/parameter is most sensitive to the pH of the waste solution, discharge rates, and the reactive surface area available for adsorption. However, as a key finding, UQ analysis also indicates that this model (and parameters) sensitivity evolves in space and time, and its understanding could be

* Corresponding author at: CONICET-IHLLA, República de Italia 730, Azul, BA 7300 Argentina. Tel.: +1 510 495 2146.
E-mail addresses: SABea@lbl.gov, SABea@faa.unicen.edu.ar (S.A. Bea), HMWainwright@lbl.gov (H. Wainwright), NSpycher@lbl.gov (N. Spycher), BFaybishenko@lbl.gov (B. Faybishenko), SSHubbard@lbl.gov (S.S. Hubbard), MILES.Denham@srnl.doe.gov (M.E. Denham).
[1] Tel.: +1 510 495 2038.
[2] Tel.: +1 510 495 2388.
[3] Tel.: +1 510 486 4852.
[4] Tel.: +1 510 486 5266.
[5] Tel.: +1 803 725 5521.

0169-7722/$ – see front matter
http://dx.doi.org/10.1016/j.jconhyd.2013.04.005

crucial to assess the temporal efficiency of a remediation strategy in contaminated sites. Results also indicate that residual U(VI) and H^+ adsorbed in the vadose zone, as well as aquifer permeability, could have a significant impact on the acidic plume long-term mobility.

1. Introduction

Nuclear weapon production during the Cold War has left groundwater contaminated at many sites in the United Sates. Low-level radioactive waste solutions were often disposed into unlined seepage basins with minimal or no engineered barriers. Nitric acid and U(VI) are typical major contaminants at such contaminated sites (e.g., Hammond et al., 2011; Lichtner and Felmy, 2003; Luo et al., 2009; Zhang et al., 2011). There have been many attempts to assess the plume migration and remedial options at these sites.

The Savannah River Site (SRS) is one of such sites where low-level radioactive waste solutions were discharged into three unlined seepage basins (at a location named the F-Area) from 1955 through about 1989 (Fig. 1). Large amount of NaOH and nitrates (Fenimore and Horton, 1972; Killian et al., 1986) were disposed in the basins throughout the history of this site. As the basin operations progressed, subsurface sediments down-gradient of the basins have been significantly altered through accelerated acid weathering (Serkiz et al., 2007). One characteristic of the SRS F-Area is the high acidity in the plume, making U(VI) highly mobile. Despite many years of active remediation, the groundwater still remains acidic, and the concentrations of U(VI) and other radionuclides are still significant (Seaman et al., 2007; Fig. 1D and E). Modeling contaminant migration at this site has been limited because of the following: (1) poor understanding of the pH effect on contaminant adsorption, due to the acidic nature of the basin waste solution, (2) the use of simplistic partition coefficient (K_d) approaches to predicting the U(VI) migration, and (3) potentially enhanced U(VI) migration associated with the transport of mobile colloidal materials (e.g., see Dai et al., 2002; Kaplan et al., 1995; Newman et al., 1993; Seaman et al., 2007). It should be noted that in the acidic pH range at the SRS-F-Area, K_d values for U(VI) could change at least five orders of magnitude (Davis et al., 2004; Dong et al., 2012).

Monitored Natural Attenuation (MNA) and Monitored Enhanced Attenuation (MEA, through a pump and treatment system) are desired closure strategies at the F-Area, assuming that an increase in pH due to uncontaminated groundwater (or alkaline solution) mixing over time with the acidic plume stimulates immobilization of U(VI) (Denham and Vangelas, 2008; Sassen et al., 2012; Zhang et al., 2011). In fact, MNA is also an attractive strategy suggested for uranium mill tailing sites (Zhu and Burden, 2001; Zhu et al., 2001). The improved understanding of the long-term effects of pH on the U(VI) adsorption behavior in the saturated and unsaturated sediments is critical to assessing the MNA (or MEA) efficacy, and needs to take into account coupled hydrodynamic and reactive transport processes.

Reactive Transport (RT) simulations for U(VI) transport using surface complexation models (SCM) have been limited by a lack of site-specific data (Zhu and Burden, 2001; Zhu et al., 2001). Davis et al. (2004) had a reasonable success simulating U(VI) reactive transport with an SCM to model U(VI) adsorption by aquifer sediments at the Naturita site, Colorado. These authors identified several sources of uncertainty associated with modeling the U(VI) adsorption, including the estimation of surface site-types and magnitude of surface area, a lack of fundamental data on the effects of competitive adsorption of common groundwater solutes, and inconsistencies that could result when combining previously published SCMs that use different electric double layer formulations.

Other experimental and numerical studies involving a radioactive acidic-plume were carried out in the Oak Ridge Reservation (ORR) in east Tennessee. In this site, the contamination plume in the groundwater extends more than 2 km along the geologic strike, and it is characterized by low pH and high concentrations of aluminum, calcium, magnesium, manganese, nitrate, sulfate, uranium and technetium (Luo et al., 2009; Zhang et al., 2010). In addition, an alkaline solution to immobilize the uranium contamination was evaluated using column experiments and numerical modeling (Zhang et al., 2011).

Because of the difficulty and apparent uncertainty in assessing the adsorption properties and mobility of U(VI) under complex geochemical conditions in groundwater, several studies have performed uncertainty quantification (UQ) related to U(VI) adsorption (e.g., Curtis et al., 2006; Hammond et al., 2011). In their UQ analysis of a one-dimensional groundwater flow domain (not including the vadose zone) at the Naturita Site, Curtis et al. (2006) identified the key processes affecting the U(VI) transport under variable geochemical conditions, including the role of hydrological parameters, and determined that the U(VI) adsorption was mostly sensitive to the alkalinity and was relatively insensitive to pH at this site where pH typically remains above 6.5–7.5. Hammond et al. (2011) conducted a UQ analysis of hydrogeological conditions affecting the U(VI) discharge into the Columbia River at the Hanford 300 Area in WA, and suggested that discharge was mostly sensitive to the global permeability distribution of the large-scale hydrogeological units. To our knowledge, there have been no RT modeling and UQ studies of U(VI) mobility in the pH range from ~3 to 5.5 (which is typical for the SRS F-Area, e.g., see Barnett et al., 2002; Dong et al., 2012), coupled with the complex hydrodynamic processes in the saturated and unsaturated (vadose) zones.

The objectives of this paper are to: (1) identify the key physical and geochemical processes that control the migration of the acidic-U(VI) plume at the SRS F-Area, with particular focus on the pH range where U(VI) is highly mobile; (2) provide a rigorous sensitivity analysis to identify the key physical and geochemical parameters controlling contaminant transport and retardation in the field and their evolution over time; and 3) provide insights about plume migration and evolution constrained by chemical and groundwater measurements. To meet these objectives, the multicomponent reactive transport model TOUGHREACT (Xu et al., 2011) was applied in combination of a new tool called AGNI UQ. AGNI UQ has recently been developed as part of the Advanced Simulation Capabilities for Environmental Management (ASCEM) project

that is building an open-source, modular, and extensible reactive transport modeling capability complete with integrated data management, visualization, UQ, parameter estimation and other toolboxes (http://ascemdoe.org; Williamson et al., 2011). This effort builds on previous numerical modeling efforts at the SRS, including large scale flow and tracer transport modeling covering areas beyond the F-Area (Flach et al., 1998; Flach, 2004), as well as smaller-scale geochemical and reactive transport modeling aimed at understanding pH buffering and U(VI) transport in the F-Area saturated zone as a function of coupled physicochemical heterogeneity or 'reactive facies' (Sassen et al., 2012; Spycher et al., 2011). This effort also complements a recent study of natural attenuation at the F-Area that integrates historical groundwater composition

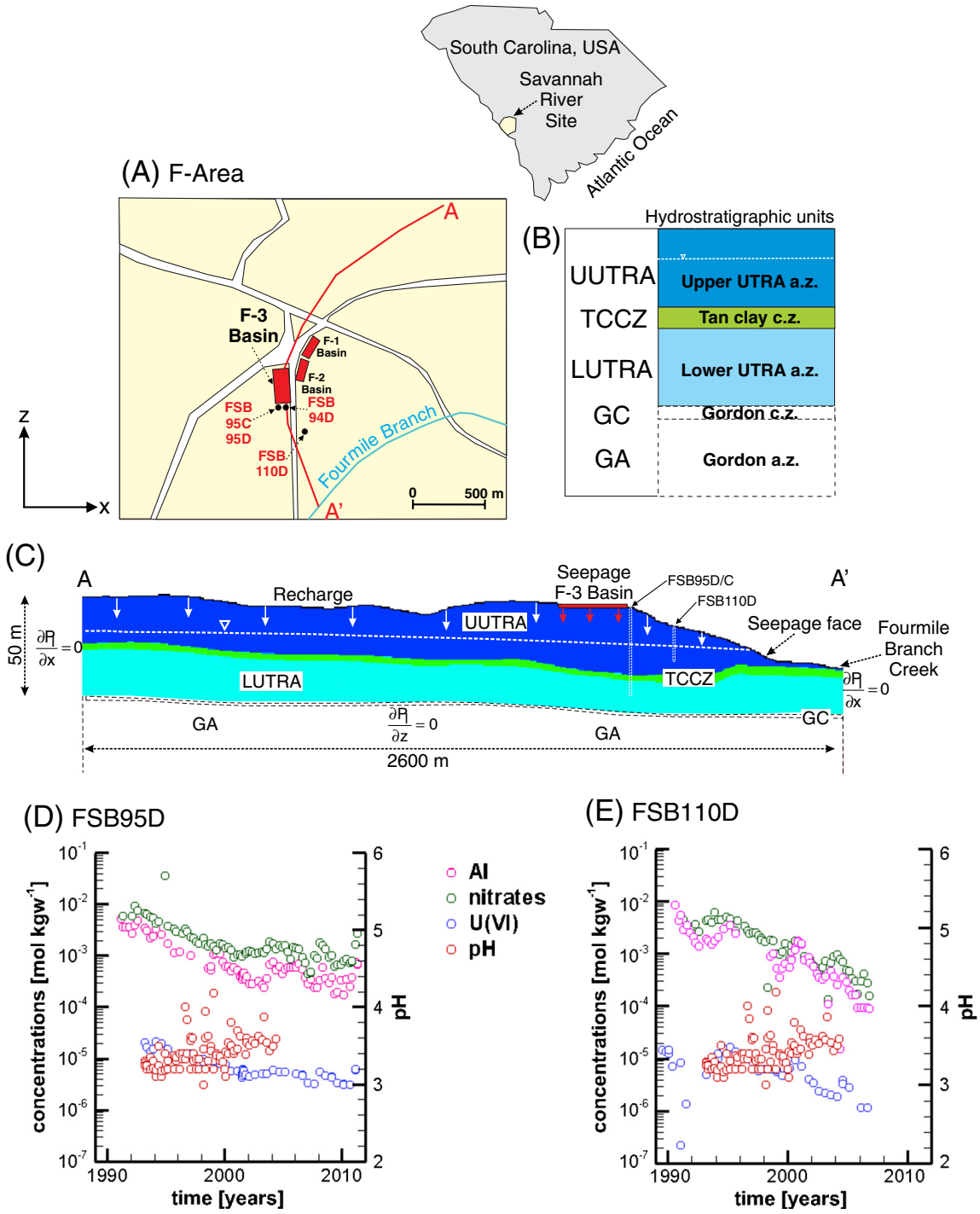

Fig. 1. (A) Location of seepage basins in the F-Area of the Savannah River Site (SRS). (B) Hydrostratigraphic units defined for the F-Area (e.g., Flach et al., 2004; Killian et al., 1986; Looney et al., 1972; Strom and Kaback, 1992). (C) 2D-cross section model domain. (D) and (E) historical concentrations of Al, nitrates, U(VI) and pH observed in groundwater at monitoring wells FSB 95D (located close to the main basin), and FSB 110D (located 300 m downstream from F3 Basin), respectively.

data with engineering analyses to examine the fate of nitrate and U(VI) at this site and the role of the vadose zone as a potential long-term source of contamination (Tokunaga et al., 2012).

2. Site description

SRS covers an area of approximately 800 km^2 located in south-central South Carolina, USA, approximately 100 mi from the Atlantic Ocean. The area experiences a temperate climate with mild winters and long summers, with an average annual rainfall of about 1.22 m and an average pan evaporation rate about 1.45 m $year^{-1}$, resulting in a suggested evaporation rate of about 1.02 to 1.17 m $year^{-1}$ and implying that the system is hydrologically balanced (Flach et al., 2004). Prior modeling efforts covering the area surrounding the seepage basins (Boltz, 1997; Flach and Harris, 1997; Flach et al., 1999; Harris et al., 2004; Sadler, 1995; Seaman et al., 2007) and nearby hydrologic budget and lysimeter studies (Cahill, 1982; Denehy and McMahon, 1985; Hubbard and Emslie, 1984; Parizek and Root, 1986) suggest an average recharge to the vadose zone from rainfall in the range of 0.15 to 0.41 m $year^{-1}$.

The site includes various facilities that were involved in producing special radioactive isotopes (e.g., plutonium and tritium, ^3H) for the U.S. nuclear weapon effort. The three SRS F-Area Seepage Basins are located in the north-central portion of the SRS (Fig. 1A). These basins, which are unlined, received ~7.1 billion liters of acidic-low-level waste solutions from processing irradiated uranium from 1955 through 1988 (e.g., see Flach et al., 2004; Killian et al., 1986). The plume currently extends from the basins ~600 m downstream, and contains a number of contaminants (e.g., $^{238}U/^{235}U$, ^3H, ^{90}Sr, nitrates). Groundwater is currently acidic, with pH values between ~3 in the center of plume and 5.4 upgradient of the basins. The sediments that underlie the F-Area have been exposed to acidic solutions for many decades (Fig. 1D and E).

The site hydrogeology has been described in detail in many site reports (e.g., Flach et al., 2004; Killian et al., 1986; Looney et al., 1972; Strom and Kaback, 1992). Sediments at the site were deposited primarily in shallow marine and fluvial environments (e.g., Gohn, 1988; Jean et al., 2004). The contaminant plume from the F-Area basin (e.g., see Sassen et al., 2012) extends within the Upper and Lower aquifers (UUTRA and LUTRA, Fig. 1B and C). The Barnwell group – including most part of both UUTRA and LUTRA – consists of two major depositional facies; Barrier Beach facies composed mostly of clean sand, and Lagoonal facies composed of sandy clay (Jean et al., 2004; Sassen et al., 2012). The major minerals identified at the site are quartz [SiO_2], kaolinite [$Al_2Si_2O_5OH_4$] and goethite [FeOOH], based on sediments samples collected from a borehole 21.7–23.7 m deep below the surface, near the contaminated F-Area of the SRS (Dong et al., 2012). The amount of other clays and carbonates is typically negligible to minor in the upper unconfined aquifer, but increases in deeper aquifers (e.g., Serkiz et al., 2007; Strom and Kaback, 1992). The two aquifers are separated by a semi-continuous lagoonal deposit known as the Tan Clay Confining Zone (TCCZ) (Jean et al, 2004). These two aquifers are hydrologically connected, judging from the piezometric head measurements. The deeper aquifer, the Gordon Aquifer, is considered to be hydrologically separated from the upper two aquifers by the continuous Gordon Confining unit.

In order to enhance MNA, a pump-and-treat remediation system began operation in 1997, and it was replaced in 2004 by a hybrid funnel-and-gate system installed about 300 m upgradient from the FMB creek. However, the enhanced attenuation (i.e., MEA) was currently chosen as an alternative remediation option, and alkaline solutions are now being injected into the subsurface near in an attempt to neutralize the acidic groundwater downgradient of the seepage basins.

3. Model development and inputs

3.1. Review of literature on U(VI) adsorption

Numerous geochemical studies over the past several decades have suggested that U(VI) adsorption onto the mineral surfaces and its mobility in groundwater depend on the geochemical conditions, mainly pH and P_{CO2} (Barnett et al., 2002; Curtis et al., 2006; Davis et al., 2004; Dong et al., 2012; Jang et al., 2007; Mahoney et al., 2009; Sherman et al., 2008; Waite et al., 1994). The adsorption process is generally nonexistent or weak in the low-pH environment (i.e., up to about pH 6), while U(VI) is strongly adsorbed and practically immobile when pH is close to neutral, except in the presence of dissolved CO_2 which forms strong carbonates complexes (e.g., Dong and Brooks, 2006).

Different mechanistic models have been proposed to account for the U(VI) retardation in the aquifer materials. For most of the metal and radionuclide risk assessments conducted by the U.S. government, reactive transport models utilize the *constant-K_d* approach (Bethke and Brady, 2000; Davis et al., 2004; U.S. EPA, 1999). However, the use of such models often leads to inadequate predictions of geochemical conditions in groundwater (Bethke and Brady, 2000; Curtis et al., 2006; Davis et al., 2004; Read et al., 1998; Zhu and Burden, 2001). In contrast to the *constant-K_d* modeling approach, surface complexation models (SCM) can describe adsorption of metal contaminants under specific geochemical conditions prevailing at a particular site (e.g., Davis et al., 2004; Dong et al., 2012; Jang et al., 2007; Kohler et al., 1996; Mahoney et al., 2009; Waite et al., 1994). Although SCM's are mostly successful in system involving a single (dominant) sorbing mineral phase (Arnold et al., 2001; Kohler et al., 1996; Waite et al., 1994), efforts have been made to use SCM's to characterize U(VI) adsorption into a mixture of minerals (Davis et al., 2004; Dong et al., 2012).

Davis et al. (2004) stated that the two major approaches for applying the SCM concept in soils and sediments are (Davis et al., 2004): (1) the Component Additivity (CA), and (2) the Generalized Composite (GC) approaches. In the former, it is assumed that a mineral assemblage is composed of a mixture of reference mineral phases, the surface chemical reactions of which are known from independent studies. In contrast, the latter GC approach assumes that one mineral component dominates adsorption. With this approach, the surface of the mineral assemblage is considered too complex to quantify in terms of contribution of individual phases to adsorption. A hybrid CA method with re-fitting of partition coefficients specific to the SRS F-Area was presented by Dong et al. (2012) to model U(VI) adsorption onto a kaolinite–goethite

assemblage, using the SCM of Sherman et al. (2008) for the adsorption of U(VI) onto goethite, and that of Heidmann et al. (2005) for U(VI) adsorption onto kaolinite.

3.2. Conceptual model of H^+ and U(VI) transport at the SRS F-Area

The natural attenuation of the acidic-U(VI) plume in the F-Area SRS is likely to be affected by the following processes: (1) adsorption/desorption of U(VI) onto/from the surface of different minerals (mainly kaolinite and goethite at this site) under different mechanisms (i.e., electrostatic surface complexation and/or ion exchange, Dong et al., 2012); (2) pH effects related to H^+ sorption and/or Al mineral dissolution and precipitation (e.g., Spycher et al., 2011); (3) mixing of the plume groundwater with clean (and higher pH) background groundwater; (4) formation of U(VI)-aqueous complexes that are more stable than the uranyl species (UO_2^{2+}) alone; and slow migration of residual H^+ and U(VI) through the vadose zone and into the groundwater.

Although high alkaline solutions with important amounts of nitrates and NaOH were periodically added to the basins (F-1 to F-2 and to F-3, Fig. 1A) during the site operations, the pH of the discharge entering the subsurface from the largest of the basins (F-3) was mostly likely fairly constant and low (Millings et al., 2012). The processes affecting the migration of acidic solutions through the vadose zone below the F-3 basin are similar to those previously evaluated with simpler models of the F-Area saturated zone (e.g., Spycher et al., 2011). These include the dissolution of the primary minerals kaolinite [$Al_2Si_2O_5(OH)_4$] and goethite [FeO(OH)]), which increase the dissolved Si, Al, Fe(III) concentrations in the plume; the potential precipitation of secondary minerals such as Al hydroxides (e.g., gibbsite [$Al(OH)_3$]) and hydroxysulfates (e.g., jurbanite [$Al(SO_4)(OH).5H_2O$] and basaluminite [$Al_4(SO_4)(OH)_{10}.5H_2O$]), and silica polymorphs (e.g., opal-CT and amorphous silica); and the adsorption of H^+ onto kaolinite, goethite, and potential secondary phases. Kaolinite (and to a lesser extent goethite) dissolution during seepage of acidic solutions (here referred to as Stage I, discharge) provides the first pH buffering mechanism in the system (with 3 moles of H^+ consumed for each mode of dissolved Al or Fe). Historical datasets of pH and U(VI) concentration fronts show that these fronts were retarded in the acidic plume compared to other more conservative components such as ^3H. Nitrate adsorption onto kaolinite also likely occurred (e.g., Heidmann et al., 2005; Table 3), although to a negligible extent relative to the elevated nitrate concentration in the discharge. The high U(VI) and H^+ concentrations in the acidic seepage solution saturated the limited sites for sorption onto kaolinite and goethite after which the plume behavior reached a stationary state.

After the basin closure (here called Stage II, capping), the acidic seepage rate to groundwater was progressively reduced, and the acidic plume started to evolve in a new equilibrium state, where the mixing processes with the uncontaminated groundwater (pH ~5.4), the desorption of H^+ from kaolinite and goethite, and the reprecipitation of kaolinite and/or other Al silicates, hydroxides, or hydroxysulfates likely controlled the pH rebound (e.g., Sassen et al., 2012; Spycher et al., 2011). U(VI) accumulated in the vadose zone underlying the basin also served as a residual source for the groundwater contamination.

3.3. Numerical model

The reactive transport code TOUGHREACT (Xu et al., 2011) was used to simulate the reactive processes discussed above. In addition, uncertainty quantification (UQ) analyses were conducted using the AGNI tool developed for ASCEM (Williamson et al., 2011) to address the sensitivity of model results to various input parameters affecting the migration of the acidic-U(VI) plume migration at the F Area. A summary of the mathematical formulation for flow and reactive solute transport is provided in the Appendix A.

4. Modeling approach

The modeling domain consists of a two-dimensional vertical cross-section about 2600 m long and 100 m deep, oriented along the plume centerline and passing through the middle of the F-3 basin (Fig. 1). This orientation essentially follows a groundwater streamline through the F-Area, as predicted previously with a larger flow model of the SRS site that extended significantly beyond the F-Area (Flach, 2004).

The four hydrostratigraphic units defined in the model consist of (Fig. 1B): (1) Upper aquifer (UUTRA); (2) Lower aquifer (LUTRA); (3) Tan Clay (TCCZ); and (4) the Gordon confining (GC) unit (e.g., Flach et al., 2004; Jean et al., 2004; Sassen et al., 2012). The interfaces/thickness among the different hydrostartigraphic units within the modeled cross-section were estimated using geostatistics on the basis of foot-by-foot cone penetrometer testing (CPT) data (Jean et al., 2004). Homogeneous geochemical and hydrogeological properties were assumed within each unit as are described below.

4.1. Hydrological properties

Average hydrological properties for each modeled hydrostratigraphic units (Table 1) were compiled from existing site investigation reports, including porosity data (Flach, 2001; Flach et al., 2004), hydraulic conductivity data from pumping and slug tests in the saturated zone (Flach et al., 2004), laboratory measurements, and capillary pressure/saturation data for the vadose zone (Phifer et al., 2006). Because the system was considered to be advective dominated, hydro-mechanical and diffusion transport processes were neglected. However, dual-domain model (DDM) could improve the model prediction as it was suggested by Flach (2001) and Flach et al. (2004) for the F and H-Areas in the SRS (H-Area is adjacent to F-Area).

4.2. Geochemical system

The geochemical system considered here builds on geochemical modeling analyses and reactive transport simulations conducted previously over smaller scales (Sassen et al., 2012; Spycher et al., 2011) together with U(VI) adsorption modeling results for F-Area sediments presented by Dong et al. (2012). The modeled system consists of fifteen mobile chemical components (i.e., U(VI), H, Al, Fe(III), Mg, Ca, Na, K, Si, Cl, TIC (Total Inorganic Carbon), SO_4, nitrates, ^3H and H_2O), four mineral surfaces for H^+ and U(VI) adsorption/exchange onto kaolinite (>kOH, $>k^-$),

Table 1
Physical model parameters used in the simulations.

Hydrostratigraphic unit	Porosity ϕ [−]	Permeability k [m^2]	α [a,b] [kg^{-1} m s^2]	n [a,c] [−]	m [c,d] [−]	S_{rl} [e] [−]	p [c] [−]
Upper aquifer (UUTRA)	0.39	5×10^{-12}	4×10^{-4}	1.37	0.27	0.18	1
Tan clay (TCCZ)	0.39	1.98×10^{-14}	5.1×10^{-5}	2	0.5	0.39	1
Lower aquifer (LUTRA)	0.39	5×10^{-12}	5.1×10^{-5}	2	0.5	0.41	1

[a] Fitted from Phifer et al. (2006).
[b] For Eq. (A4).
[c] For Eq. (A5).
[d] Computed using Eq. (A7).
[e] For Eq. (A8).

and goethite (>FeOH) and quartz (>qz). Modeled aqueous and surface complexes are assumed to form at equilibrium (Tables 2 and 3, respectively).

The dissolution and precipitation of primary minerals (i.e., quartz, kaolinite and goethite) were modeled using kinetic rate expressions derived from the literature (Table 5). Gibbsite, jurbanite, basaluminite, opal-CT and schoepite [$(UO_3)\cdot 2H_2O$] are the species that potentially form when the plume interacts with the solids. Their equilibrium constants are given in Table 4, whereas their kinetic parameters are shown in Table 5.

Yang and Steefel (2008) presented an asymmetric kinetic dissolution/precipitation rate law for kaolinite at ambient temperature and pressure and low pH (~4) on the basis of experimental measurements. These authors showed that the Transition State Theory (TST) could describe kaolinite dissolution and initial precipitation close to equilibrium, but not precipitation away from equilibrium, which showed a linear dependence on solution saturation state, generally consistent with a two-dimensional nucleation growth mechanism. The form of Yang and Steefel's rate law for kaolinite is not currently implemented into the TOUGHREACT simulator. For this reason, the rates measured by these authors were fitted (approximately) using the TST function of the simulator with asymmetric exponents on the affinity term (Table 5). The rate behavior with pH was considered by combining the rates measured by Yang and Steefel (2008) at pH ~4 with pH dependence data reported by Palandri and Kharaka (2004).

Regarding the kinetic dissolution of quartz, we selected the data from Tester et al. (1994) for the neutral pH mechanism, because the authors were able to correlate consistently their experimental results with the results of other sources at ambient temperatures. Because of extremely slow quartz precipitation kinetics at low temperatures, only dissolution is considered. Secondary fast forming silica polymorphs (opal-CT) are allowed to form (Table 5). Note that amorphous silica is also allowed to form but never precipitates as long as less soluble opal-CT is present.

We assume that the initial mineralogy is composed of a mixture of quartz, kaolinite and goethite (Table 6). The volumetric fraction occupied by each mineral is calculated from Al:Fe ratio measured in the samples from the F-Area (Sassen et al., 2012). We consider that the molar Al:Fe ratio is a proxy for the kaolinite:goethite molar ratio, assuming that all measured Fe by XRF (X-ray Fluorescence) is from goethite and all measured Al is from kaolinite (i.e., neglecting potential Al substitution in goethite).

The chemical compositions for the initial and boundary solutions (as presented further below) are listed in Table 7. The initial pore water composition was determined from analyses of water samples collected upgradient of the F-Area basins (Fig. 1A), then modified to reflect total concentrations of Al, Fe(III) and Si controlled by equilibrium with kaolinite,

Table 2
Aqueous complexes considered in the simulations.

Reaction	$\log_{10}$ K (25 °C)	Ref.
$OH^- \leftrightarrow H_2O - H^+$	13.99	(1)
$AlOH^{2+} \leftrightarrow Al^{3+} + H_2O - H^+$	5	(1)
$Al(OH)_2^+ \leftrightarrow Al^{3+} + 2H_2O - 2H^+$	10.1	(1)
$Al(OH)_3(aq) \leftrightarrow Al^{3+} + 3H_2O - 3H^+$	16.9	(1)
$Al(OH)_4^- \leftrightarrow Al^{3+} + 4H_2O - 4H^+$	22.7	(1)
$CaOH^+ \leftrightarrow Ca^{2+} + H_2O - H^+$	12.83	(1)
$CaHCO_3^+ \leftrightarrow HCO_3^- + Ca^{2+}$	−1.04	(1)
$CaCO_3(aq) \leftrightarrow HCO_3^- + Ca^{2+} - H^+$	7	(1)
$CO_3^{2-} \leftrightarrow HCO_3^- - H^+$	10.32	(1)
$CO_2(aq) \leftrightarrow HCO_3^- - H_2O + H^+$	−6.34	(1)
$H_2CO_3(aq) \leftrightarrow HCO_3^- + H^+$	−6.3	(1)
$NaCO_3^- \leftrightarrow Na^+ + HCO_3^- - H^+$	9.81	(1)
$NaHCO_3(aq) \leftrightarrow Na^+ + HCO_3^-$	−0.15	(1)
$NaOH(aq) \leftrightarrow Na^+ + H_2O - H^+$	14.2	(1)
$MgCO_3(aq) \leftrightarrow HCO_3^- + Mg^{2+} - H^+$	7.35	(1)
$Mg(OH)^+ \leftrightarrow Mg^{2+} + H_2O - H^+$	11.68	(1)
$MgHCO_3^+ \leftrightarrow Mg^{2+} + HCO_3^-$	−1.04	(1)
$(UO_2)_2(OH)_2^{2+} \leftrightarrow 2UO_2^{2+} + 2H_2O - 2H^+$	5.62	(1)
$(UO_2)_2CO_3(OH)_3^- \leftrightarrow HCO_3^- - 4H^+ + 2UO_2^{2+} + 3H_2O$	11.18	(1)
$(UO_2)_2OH^{3+} \leftrightarrow 2UO_2^{2+} + H_2O - H^+$	2.7	(1)
$(UO_2)_3(CO_3)_6^{6-} \leftrightarrow 6HCO_3^- - 6H^+ + 3UO_2^{2+}$	7.97	(1)
$(UO_2)_3(OH)_4^{2+} \leftrightarrow 3UO_2^{2+} + 4H_2O - 4H^+$	11.9	(1)
$UO_2(OH)_4^{2-} \leftrightarrow UO_2^{2+} + 4H_2O - 4H^+$	32.4	(1)
$(UO_2)_3(OH)_5^+ \leftrightarrow 3UO_2^{2+} + 5H_2O - 5H^+$	15.55	(1)
$(UO_2)_3(OH)_7^- \leftrightarrow 3UO_2^{2+} + 7H_2O - 7H^+$	32.2	(1)
$(UO_2)_3O(OH)_2(HCO_3)^+ \leftrightarrow HCO_3^- - 4H^+ + 3UO_2^{2+} + 3H_2O$	9.68	(1)
$(UO_2)_4(OH)_7^+ \leftrightarrow 4UO_2^{2+} + 7H_2O - 7H^+$	21.9	(1)
$UO_2NO_3^+ \leftrightarrow UO_2^{2+} + NO_3^-$	−0.3	(1)
$UO_2(OH)^+ \leftrightarrow UO_2^{2+} + H_2O$	5.25	(1)
$UO_2(OH)_2(aq) \leftrightarrow UO_2^{2+} + 2H_2O - 2H^+$	12.15	(1)
$UO_2(OH)_3^- \leftrightarrow UO_2^{2+} + 3H_2O - 3H^+$	20.25	(1)
$UO_2CO_3(aq) \leftrightarrow UO_2^{2+} + HCO_3^- - H^+$	0.39	(1)
$UO_2(CO_3)_2^{2-} \leftrightarrow UO_2^{2+} + 2HCO_3^- - 2H^+$	4.05	(1)
$UO_2(CO_3)_3^{4-} \leftrightarrow UO_2^{2+} + 3HCO_3^- - 3H^+$	9.14	(1)
$CaUO_2(CO_3)_3^{2-} \leftrightarrow Ca^{2+} + UO_2^{2+} + 3HCO_3^- - 3H^+$	3.8	(1)
$Ca_2UO_2(CO_3)_3(aq) \leftrightarrow 2Ca^{2+} + UO_2^{2+} + 3HCO_3^- - 3H^+$	0.29	(1)
$MgUO_2(CO_3)_3^{2-} \leftrightarrow Mg^{2+} + UO_2^{2+} + 3HCO_3^- - 3H^+$	5.19	(1)
$UO_2SiO(OH)_3^+ \leftrightarrow SiO_2(aq) + UO_2^{2+} + 2H_2O - H^+$	2.48	(1)

[(1)] Dong et al. (2012), including data for U species originally from Guillaumont et al. (2003).

Table 3
Surface complexation and cation-exchange reactions considered in the simulations.

Reaction	$\log_{10}$ K (25 °C)	Ref.
(1)On kaolinite		
$(>\text{k-OH})_2UO_2^+ \leftrightarrow 2 >\text{k-OH}^{-0.5} + UO_2^{2+}$	−5.3	(5)
$(>\text{k-OH})_2UO_2CO_3^- \leftrightarrow 2 >\text{k-OH}^{-0.5} + UO_2^{2+} + HCO_3^- - H^+$	−6.2	(5)
$>\text{k-OH}_2^{+0.5} \leftrightarrow >\text{k-OH}^{-0.5} + H^+$	−4.9	(5)
$>\text{k-OHNa}^{+0.5} \leftrightarrow >\text{k-OH}^{-0.5} + Na^+$	2.1	(5)
$>\text{k-OH}_2NO_3^{0.5} \leftrightarrow >\text{k-OH}^{-0.5} + H^+ + NO_3^-$	−4.9	(5)
(2)On kaolinite		
$>\text{k}_2UO_2 \leftrightarrow 2 >\text{k}^- + UO_2^{2+}$	−7.1	(5)
$>\text{kNa} \leftrightarrow >\text{k}^- + Na^+$	−2.9	(5)
$>\text{kH} \leftrightarrow >\text{k}^- + H^+$	−4.5	(5)
$>\text{k}_2Ca \leftrightarrow 2 >\text{k}^- + Ca^{2+}$	−6.8	(5)
$>\text{k}_3Al \leftrightarrow 3 >\text{k}^- + Al^{3+}$	−8	(5)
(3)On goethite		
$(>\text{Fe-OH})_2UO_2^+ \leftrightarrow 2 >\text{Fe-OH}^{-0.5} + UO_2^{2+}$	−14.11	(5)
$(>\text{Fe-OH})_2UO_2CO_3^- \leftrightarrow 2 >\text{Fe-OH}^{-0.5} + UO_2^{2+} + HCO_3^- - H^+$	−4.35	(5)
$>\text{Fe-OH}_2^{+0.5} \leftrightarrow >\text{Fe-OH}^{-0.5} + H^+$	−9.18	(5)
$(>\text{Fe-OH})_2CO_2^- \leftrightarrow 2 >\text{Fe-OH}^{-0.5} + HCO_3^- - 2H_2O + H^+$	−12.23	(5)
$>\text{Fe-OCO}_2Na^{-0.5} \leftrightarrow >\text{Fe-OH}^{-0.5} + HCO_3^- - H_2O$	−3.28	(5)
(4)On quartz		
$>\text{qz-OH}_2^+ \leftrightarrow >\text{qz-OH} + H^+$	1.1	(6)
$>\text{qz-O}^- \leftrightarrow >\text{qz-OH} - H^+$	8.1	(6)
$>\text{qz-ONa} \leftrightarrow >\text{qz-OH} - H^+ + Na^+$	6.8	(7)

(1)Diffuse-layer, Gouy–Chapman, edge site density 2.3 [sites nm^{-2}] (Dong et al., 2012; Heidmann et al., 2005).
(2)Cation-exchange, Gaines–Thomas convention, exchange site density 0.28 [sites nm^{-2}] (Dong et al., 2012; Heidmann et al., 2005).
(3)Diffuse-layer, Gouy–Chapman, edge site density 3 [sites nm^{-2}] (Dong et al., 2012; Sherman et al., 2008).
(4)Diffuse-layer, Gouy–Chapman, site density 10 [sites nm^{-2}] (Landry et al., 2009).
(5)Dong et al. (2012).
(6)Sverjensky and Sahai (1996).
(7)Landry et al. (2009).

goethite and quartz, respectively. The chemical composition of the natural recharge solution (i.e., infiltration of rainwater) was assumed the same as the background groundwater composition, circumventing the need to account for potentially complex and uncertain interactions between rain-water and surface/near-surface soils and sediments. The acidic-seepage solution composition was modified on the base of the average composition proposed by Killian et al. (1986). The bulk solutions were equilibrated with the atmospheric $CO_2(g)$ ($P_{CO2(g)} = 10^{-3.5}$ atm, Table 7).

4.3. Boundary and initial conditions

We imposed impervious boundary conditions for flow along the two vertical sides of the 2D-cross section (Fig. 1C). This is consistent with groundwater divides defined in the watershed based on the water-table measurements and previous numerical efforts in the F-Area (e.g., Flach, 2004) (Fig. 1C). An impervious flow boundary is also assigned at the bottom of LUTRA, because the confining unit at this location is highly clayey and continuous. Estimated fluxes from rainfall records and runoff estimations (Flach et al., 2004) are used to prescribe a fixed (average) infiltration at the top of the modeled domain to simulate natural recharge (0.15 $m^3\ m^{-2}\ year^{-1}$). A transient seepage rate is then imposed at the location of the F-3 basin (Table 8) based on historical data (Flach, 2001), corresponding to an average rate of ~3500 kgw $m^{-2}\ year^{-1}$ (~3.19×10^9 total kgw from Basin F-3) during the 35-year operation of the basins.

In the present model, the water table is not fixed a priori, because it is controlled by the imposed recharge fluxes on the top and the outflow through the upper right-most grid blocks of the model, which coincide with a seep-line and creek (the Fourmile Branch or FMB) located downgradient of the basins (Fig. 1C). The seepage face is simulated by including a fictitious grid-block in the numerical domain that represents atmosphere with a fixed atmospheric pressure (P_{atm}, M $L^{-1}\ T^{-2}$), and that is connected with the model grid blocks located in the topographic surface. The Darcy fluxes (q_s, [M $L^{-2}\ T^{-1}$]) between the atmosphere and surface grid blocks are evaluated as (upstream weighted):

$$q_s = -\rho_l \frac{\mathbf{K} k_r}{\mu_l} \nabla P_c \quad P_l > P_{atm}$$
$$k_r = 0, q_s = 0 \quad P_l <= P_{atm} \tag{1}$$

where ρ_l is the fluid density [M L^{-3}], μ_l is the dynamic fluid viscosity [M $L^{-1}\ T^{-1}$], **K** is the permeability in the porous medium close to the topographic surface [L^2], k_r is the relative permeability [−], and P_c, P_l and P_{atm} are the capillary, liquid and atmospheric pressures, respectively. Note that only positive flux (i.e., outflow) is allowed with this approach.

Initial steady-state flow conditions are computed before starting the RT simulations, imposing a hydrostatic pressure distribution throughout the modeled domain.

For the transport and chemistry boundary conditions, we prescribed mass fluxes based on the background chemical composition (Solution 3, Table 7) in the natural recharge, whereas the acidic-seepage solution composition is imposed only along the footprint of the F-3 basin (Solution 2, Table 7).

4.4. Modeling scenario

A total time period of about 60 years was simulated, corresponding to a time window from 1955 to 2015. Despite

Table 4
Mineral dissolution/precipitation reactions considered in the simulations.

Reaction	$\log_{10}$ K (25 °C)	Ref.
Quartz $\leftrightarrow SiO_2(aq)$	−3.7501	(1)
Kaolinite $\leftrightarrow 2Al^{3+} + 2SiO_2(aq) + 5H_2O - 6H^+$	7.57	(2)
Goethite $\leftrightarrow Fe^{3+} + 2H_2O - 3H^+$	0.1758	
Schoepite $\leftrightarrow UO_2^{2+} + 3H_2O - 2H^+$	4.8443	(1)
Gibbsite $\leftrightarrow Al^{3+} + 3H_2O - 3H^+$	7.738	(3)
Jurbanite $\leftrightarrow Al^{3+} + SO_4^{2-} + 6H_2O - H^+$	−3.8	(4)
Basalumini te $\leftrightarrow 4Al^{3+} + SO_4^{2-} + 15H_2O - 10H^+$	22.251	(4)
Opal $\leftrightarrow SiO_2(aq)$	−3.005	(5)

(1)SNL (2007), within error margins of Guillaumont et al. (2003).
(2)Yang and Steefel (2008).
(3)Pokrovskii and Helgeson (1995).
(4)Nordstrom (1982).
(5)Sonnenthal and Spycher (2000).

Table 5
Kinetic parameters used in the simulations.

Mechanism[a]	Neutral	Acid		Base			
Mineral	kn_i	ka_i	p	kb_i	q	η	θ
Quartz [b,e,f]	$10^{-13.345}$	–	–	–	–	1	1
Kaolinite[c] (diss.)	$10^{-12.967}$	$10^{-11.098}$	0.777	$10^{-16.839}$	−0.472	1	0.5
Kaolinite[c] (prec.)	$10^{-14.126}$	$10^{-12.256}$	0.777	$10^{-17.996}$	−0.472	1	0.33
Goethite[b]	$10^{-7.94}$	–	–	–	–	1	1
Schoepite	Equilibrium						
Gibbsite[b]	$10^{-11.5}$	$10^{-7.65}$	0.992	$10^{-16.65}$	−0.784	1	1
Jurbanite[d]	10^{-8}	–	–	–	–	1	1
Basaluminite[d]	10^{-8}	–	–	–	–	1	1
Opal[g] (diss.)	$10^{-12.135}$	–	–	–	–	1	1
Opal[h] (prec.)	$10^{-9.135}$	–	–	–	–	1	1

[a] Computed as $R_i = [kn_i + ka_i a_{H+}^{p} + kb_i a_{H+}^{q}](1 - \Omega^{\eta})^{\theta}$.
[b] Palandri and Kharaka (2004).
[c] Fitted from Yang and Steefel (2008) using the pH dependency parameters from Palandri and Kharaka (2004) (see text).
[d] Estimated fast rate.
[e] Tester et al. (1994).
[f] Dissolution is only allowed.
[g] Rimstidt and Barnes (1980) (for amorphous silica).
[h] Estimated three orders of magnitude faster than for dissolution.

the fact that a recirculation system involving a base addition is currently being implemented in the F-Area SRS, close to FMB (see "Site description" section), it was not included in this work because we aim to identify and isolate the key natural processes that attenuate the plume. However, the present reactive transport model and uncertainty quantification analyses presented here could be the basis for future works to evaluate this remediation strategy in particular and others in the site.

The modeling scenario covers two stages of the F-area historical operations (Killian et al., 1986): (1) Stage I (1955–1988), the period during which waste disposal was active, simulating seepage of the acidic-U(VI) solution from the F-3 basin through the vadose zone, and (2) Stage II (1989–2015), the post closure period when the basins were capped after solidification, and during which seepage from the basin into the vadose zone is assumed to have stopped.

4.5. Flow model calibration

The present flow model was calibrated to obtain the best fit of historical measurements of ^3H concentrations within the F-Area and into the FMB creek. This area has been monitored since 1955, which provided an extensive dataset that allows us to develop a realistic numerical model and to compare the results with observed data (Flach, 2001). Various

Table 6
Initial mineral volumetric fraction distributions considered in the simulations.

Mineral	wt.% [−]	Vol. frac. [−]	Surface area [$m^2\ g^{-1}$]	Density [$g\ cm^{-3}$]
Quartz	94.5[a]	0.9496	0.14	2.648
Kaolinite	4.015[a]	0.0412	20.71[a]	2.594
Goethite	1.485[a]	0.0093	16.22[a]	4.268
Schoepite	0	0	Equilibrium	4.874
Gibbsite	0	0	120	2.44
Basaluminite	0	0	1	2.119
Opal	0	0	200	2.072
Jurbanite	0	0	1	1.789

[a] Dong et al. (2012).

Table 7
Chemical composition for the background and seepage solutions.

Component	Solutions 1 and 3	Solution 2[a]	Units
pH	5.4	2.05	[−]
Na	2.78×10^{-4}	6.82×10^{-5}	[mol kgw^{-1}]
Cl	9.98×10^{-3}[b]	3.39×10^{-5}	[mol kgw^{-1}]
TIC[c]	1.23×10^{-5}	1.09×10^{-5}	[mol kgw^{-1}]
Al	3.09×10^{-8}	10^{-8}	[mol kgw^{-1}]
Fe(III)	2.92×10^{-16}	2.75×10^{-6}	[mol kgw^{-1}]
K	3.32×10^{-5}	1.72×10^{-6}	[mol kgw^{-1}]
Ca	10^{-5}	10^{-5}	[mol kgw^{-1}]
Mg	5.35×10^{-3}	2.47×10^{-6}	[mol kgw^{-1}]
U(VI)	1.25×10^{-10}[d]	3.01×10^{-5}	[mol kgw^{-1}]
Nitrates	10^{-3}	10^{-2}	[mol kgw^{-1}]
SO_4	2.25×10^{-5}	4.8×10^{-5}	[mol kgw^{-1}]
$SiO_2(aq)$	1.77×10^{-4}	1.18×10^{-4}	[mol kgw^{-1}]
^3H	10^{-15}	2.17×10^{-9}[e]	[mol kgw^{-1}]
Ionic strength	1.64×10^{-2}	1.02×10^{-2}	[mol kgw^{-1}]
$P_{CO2(g)}$	$10^{-3.5}$	$10^{-3.5}$	[atm]
Mineral saturation indices			
SI_{quartz}	0	−0.17	[−]
$SI_{kaolinite}$	0	−18.42	[−]
$SI_{goethite}$	0	0	[−]
$SI_{schoepite}$	−4.5	−5.46	[−]
$SI_{basaluminite}$	−7.63	−35.89	[−]
$SI_{gibbsite}$	−0.17	−9	[−]
$SI_{jurbanite}$	−4.29	−6.05	[−]
SI_{opal}	−0.74	−0.92	[−]

[a] Based on Killian et al. (1986).
[b] Calculated as electric charge balance.
[c] Total inorganic carbon.
[d] Calculated for an U(VI) in the solid sediment of about 0.1 [μg g^{-1}] from measurements.
[e] Average concentration computed as $c_{av} = \sum c_i Q_i / \sum Q_i$. The summatories are over 33 years of the data shown in Table 8. Q_i and c_i are the seepage rate (kgw m^{-2} $year^{-1}$) and ^3H concentration (mol kgw^{-1}) for the i^{th} year, respectively.

attributes of the available ^{3}H dataset were considered, including cumulative ^{3}H activity discharged to F-3 Basin, plume arrival time and ^{3}H fluxes at the FMB creek, and plume attenuation due to closure of the seepage basins in 1988. Uncertain input parameters including natural recharge and permeabilities in the UUTRA and LUTRA units were manually adjusted to best reproduce the historical ^{3}H data (Fig. 4), including the cumulative ^{3}H curve (Fig. 4A) and ^{3}H activity fluxes into the FMB creek (Fig. 4B). The total ^{3}H plume transit time was 9 years, with residence times of 3 years in the vadose zone, and 6 years through the UUTRA and LUTRA units. It should be noted that observed ^{3}H fluxes into the FMB creek could not be reproduced by the model without considering flow in the LUTRA units, pointing to importance of considering this deeper unit for predictive work at the F-Area.

5. Modeling results

5.1. Base case simulation

The water-table position and flow streamlines predicted through the vadose zone and aquifers at different times are shown in Fig. 2. Before the basin closure (i.e., during Stage I), the groundwater flow was driven in large part by recharge from the F-Area basins and by discharge through the seepage-face zone into the FMB creek. Despite the low permeability of the Tan clay unit (TCCZ), leakage from the UUTRA to the LUTRA is predicted to take place over most of the flow domain, except away from the basins in the vicinity of the FMB creek, where the flow is upward through these units as the result of discharge to this area (Fig. 2). Model results also show that the water-table progressively rises below the basin during Stage I, and the important seepage rate disturbs the natural flow in the UUTRA and LUTRA units (Fig. 2A, B, C and D) during this time period.

The acidic solution dissolves kaolinite beneath the F-3 basin, delaying the pH decrease (i.e., being the first buffering mechanism in the system), and raising the predicted Al and Si concentrations in the pore water, i.e.:

$$Al_2Si_2O_5(OH)_4(s) + 6H^+ \leftrightarrow 2Al^{3+} + 2SiO_2 + 5H_2O \qquad \text{Reaction1}$$

As a result, opal-CT is predicted to precipitate below the basin, while Al is transported under acidic conditions as the plume migrates downstream. Gibbsite is predicted to form only at the plume front where the activity of silica remains low and pH is higher from mixing with uncontaminated groundwater (pH ~5.4). Because kaolinite dissolution under the basin brings the plume close to equilibrium with this mineral at this location, continued dissolution further downgradient cannot take place. Instead, kaolinite is predicted to re-precipitate away from the basin (e.g., see Fig. 3A, 1985), which delays the neutralization of the plume by uncontaminated groundwater at the plume front (i.e., precipitation of kaolinite tends to drive pH down by producing H^+; Reaction 1). These modeling results are consistent with earlier work considering only the saturated zone and a similar geochemical system (Spycher et al., 2011).

The modeling results suggest the formation of at least three concentration fronts. The first one is related to nitrate and ^{3}H concentrations, the most conservative species, and the other two are related to the low pH and high U(VI) concentration (i.e., coincident with the gibbsite/kaolinite and kaolinite precipitation fronts, respectively, see Figs. 3D, 4C, D and E). The pH and U(VI) fronts are retarded as they are affected by the adsorption (and exchange) processes onto kaolinite and goethite. Limited sites for adsorption/exchange are saturated by the elevated H^+ and U(VI) loading, so that their concentrations eventually reach a steady state (Fig. 4C, D and E).

During Stage II, after the basin closure and capping, the seepage from the basin is assumed to stop, causing significant changes in the hydraulic and geochemical processes (Fig. 3). From this time on, mixing of the plume with the uncontaminated groundwater is the dominant process (Fig. 2E and F). The pH values progressively start to rebound as the acidic plume mixes with uncontaminated groundwater and the migration of H^+ from the vadose zone is significantly diminished (Figs. 3E, F; 4C, D and E). However the pH rebound is impeded by H^+ desorption from kaolinite and goethite, and the precipitation of Al silicates and possibly hydroxysulfates (e.g., Gu et al., 2003; Spycher et al., 2011; Zhu et al., 2001). The U(VI) transport and evolution

Table 8
Seepage rate and ^{3}H source for the F-Area.

Year	F-3 basin[a] seepage rate (kgw m^{-2} year^{-1})	Net concentrations[a,b] for ^{3}H discharged to the F-3 basin (mol kgw^{-1})
1955	1264.3	2.11×10^{-10}
1956	2528.8	1.06×10^{-10}
1957	1448.6	1.84×10^{-10}
1958	989.7	0
1959	1850.8	2.9×10^{-9}
1960	3802.0	2×10^{-9}
1961	2276.2	4×10^{-9}
1962	4544.6	3.62×10^{-9}
1963	3930.1	3.98×10^{-9}
1964	5491.1	3.58×10^{-9}
1965	2769.1	5.31×10^{-9}
1966	2910.3	6.26×10^{-9}
1967	3051.5	3.56×10^{-9}
1968	3305.1	3.86×10^{-9}
1969	5096.3	2.09×10^{-9}
1970	4989.1	2×10^{-9}
1971	3211.0	1.35×10^{-9}
1972	3992.8	1.61×10^{-9}
1973	5438.8	2×10^{-9}
1974	3417.6	2×10^{-9}
1975	2059.2	1.63×10^{-9}
1976	4390.3	1.25×10^{-9}
1977	3830.7	9.33×10^{-10}
1978	4039.9	1.07×10^{-9}
1979	4994.3	1.09×10^{-9}
1980	5057.1	9.59×10^{-10}
1981	7081.0	9.75×10^{-10}
1982	3315.6	1.25×10^{-9}
1983	1927.7	3.54×10^{-9}
1984	3051.5	2.79×10^{-9}
1985	3919.6	2.3×10^{-9}
1986	4275.2	2.18×10^{-9}
1987	3138.6[c]	1.72×10^{-9}
1988	2001.9	1.43×10^{-9}

[a] Computed from data recompiled in Flach (2001).
[b] Values scaled for a factor of 0.7 to account the ^{3}H released to the atmosphere (e.g., see Flach et al., 2004).
[c] Computed as a lineal interpolation between years 1986–1988.

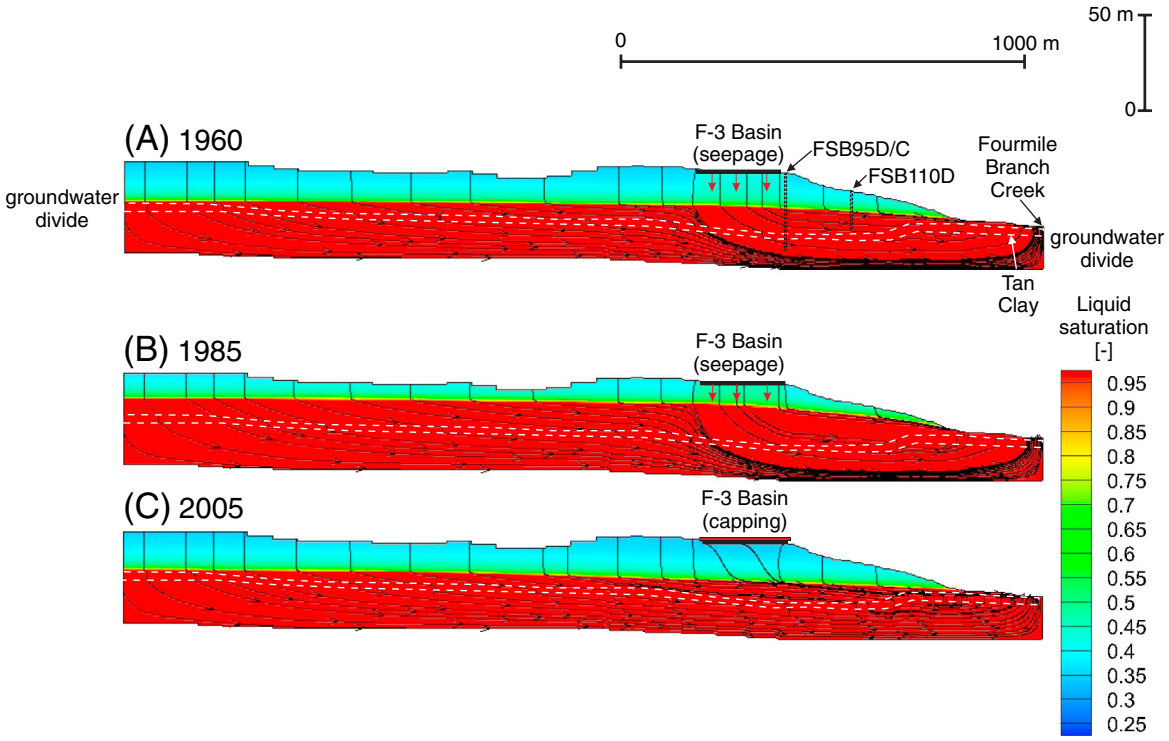

Fig. 2. Predicted water-table position in 1960 (A) and 1985 (B) prior to closure (Stage I), and in 2005 (C) post closure (Stage II). Dashed white line indicates the boundaries of the Tan Clay unit (TCCZ unit in Fig. 1). Seepage from the basin is modeled to start in 1955 (time = 0) and to end in 1988.

depends in part on pH, which in turn affects K_d values (Fig. 5A and B). In fact, in the typical pH range for the F-Area (pH ~3.5–5.4), K_d varies almost four orders of magnitude (Fig. 5A and B). However, because pH in the bulk of the plume is predicted to remain buffered to low values for decades, dilution from mixing with background water at the plume trailing edge (resulting from the high pore velocity in the saturated zone) appears to be the driving means of U(VI) attenuation in the short term.

The spatial variations of the U(VI) surface complexation onto kaolinite and goethite also depend on the spatial variability of

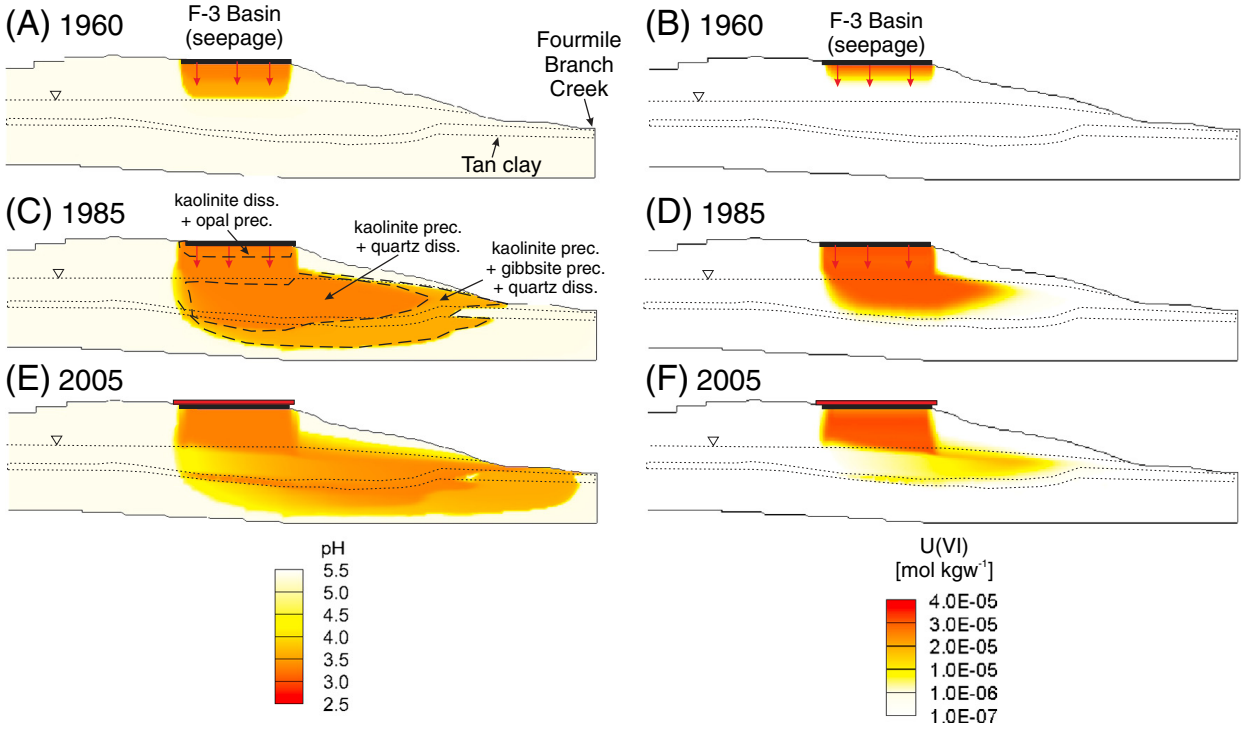

Fig. 3. Reactive transport simulations: predicted pH and U(VI) distributions in 1960 (A and B) and in 1985 (C and D) prior to closure (Stage I); and in 2005 (E and F) post closure (Stage II). Seepage from the basin is modeled to start in 1955 (time = 0) and to end in 1988.

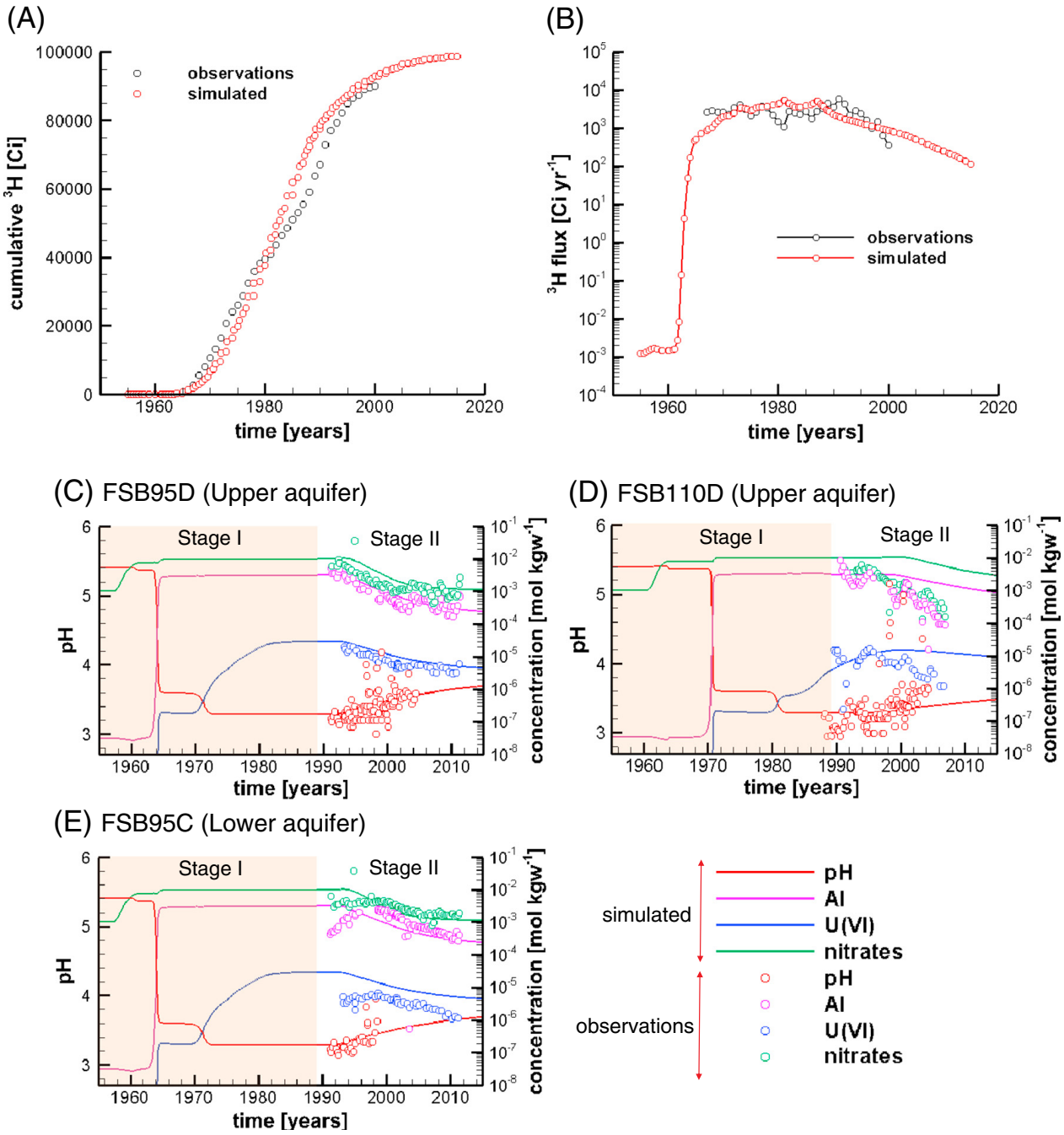

Fig. 4. Reactive transport simulation: (A) and (B) cumulative and ^{3}H fluxes in the Fourmile Branch Creek. (C), (D) and (E) breakthrough curves (BTC) for U(VI), Al, nitrates concentrations and pH at monitoring wells FSB95D, FSB110D and FSB95C, respectively (their locations are shown in Fig. 1A).

pH and U(VI) concentrations, as illustrated by a transect along the acidic plume in Fig. 5C. Exchanged-U(VI) ($>k_2UO_2$) onto edge sites of kaolinite is dominant in the bulk of the acidic plume. However, bidentate surface complexes onto goethite and kaolinite [i.e., $(>Fe\text{–}OH)_2UO_2^+$ and $(>k\text{-}OH)_2UO_2^+$, respectively] are the dominant species on the edge of the acidic plume and the uncontaminated zones. U(VI)-carbonates bidentate carbonate complexes onto goethite and kaolinite [i.e., $(>Fe\text{–}OH)_2UO_2\text{-}CO_3^-$ and $(>k\text{-}OH)_2UO_2CO_3^-$, respectively] have a minor importance in this system because of the acidic pH and low dissolved CO_2 content (e.g., Dong et al., 2012).

After the basin closure, because of the accumulation of liquids and contaminants in the vadose zone below the F-3 basin (Fig. 2E and F), pH remains low and U(VI) concentrations high (Fig. 3E, F). Therefore, the vadose zone below the basin appears to act as a long-term contaminant source for the groundwater. It should be noted, however, that previous reactive transport simulations of only the saturated zone (thus ignoring effects of residual concentrations in the vadose zone, Spycher et al., 2011) predicted the pH to remain buffered to low values for decades because of H^+ desorption and Al mineral precipitation alone (i.e., without an H^+ source from the vadose zone). The same mechanisms apply here as well, and the impact of residual H^+ from the vadose zone on pH rebound appear to be secondary to effect of desorption and mineral precipitation. After closure, the nitrate and Al concentrations in

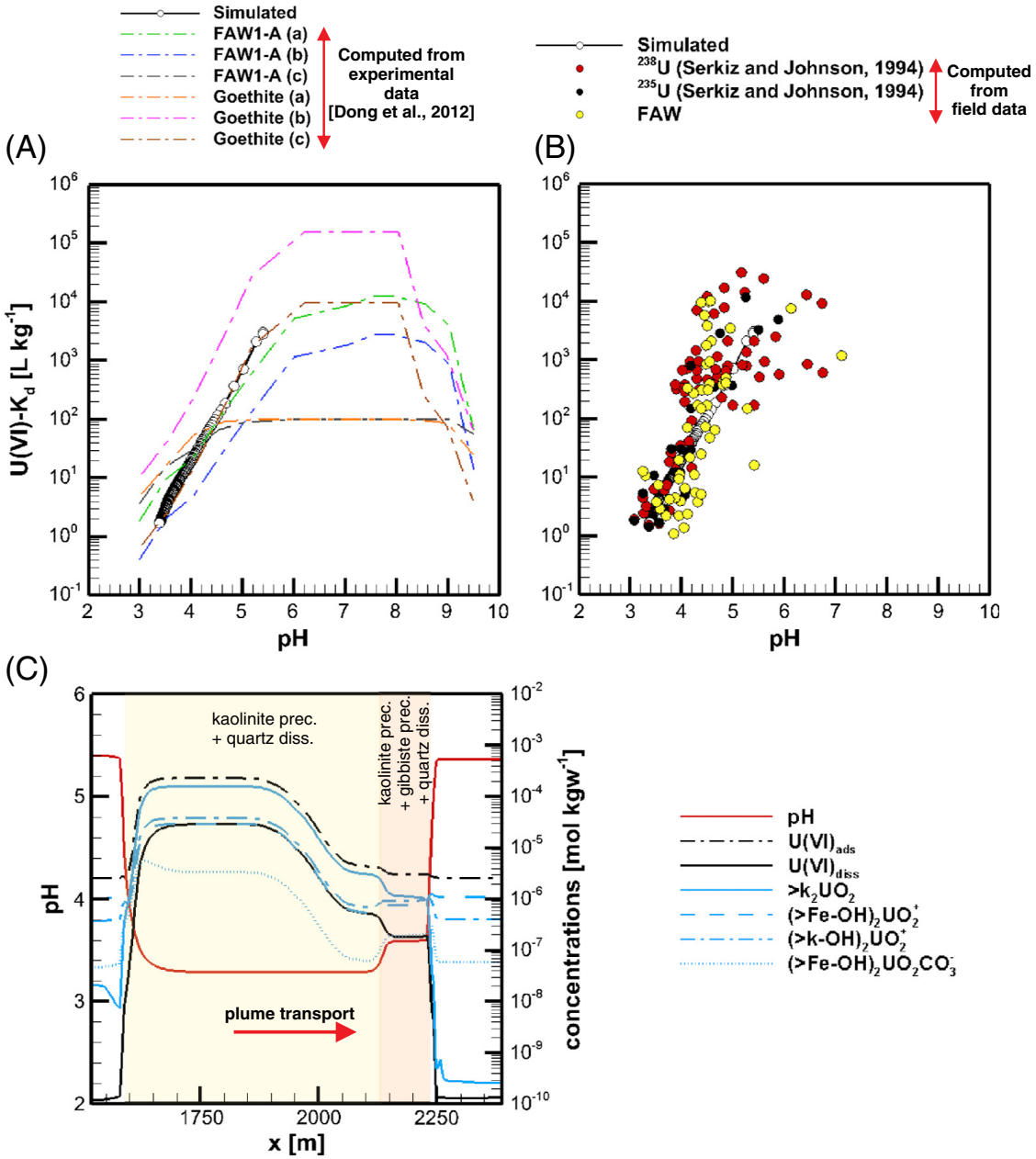

Fig. 5. Reactive transport simulations: simulated U(VI) sorption isotherms (as K_d values) compared with: (A) data calculated from Dong et al. (2012), (B) field measurements from several sources as shown (Serkiz and Johnson, 1994). (C) Predicted pH, U(VI) total concentrations and U(VI) surface complexes onto kaolinite and goethite along a horizontal transect of the modeled plume (at ~25 m depth).

groundwater are predicted to decrease continuously as the discharge of waste comes to an end and the interaction between the acidic-plume and subsurface materials diminishes (Fig. 4C, D and E).

6. Uncertainty quantification (Uq) analysis

UQ analyses were conducted to evaluate the model result sensitivity to important input parameters and the effect of parameter uncertainty on the predicted migration of the acidic-U(VI) plume. These analyses were also performed to demonstrate new UQ capabilities developed as part of the Advanced Simulation Capability for Environmental Management (ASCEM) framework (Williamson et al., 2011), for which the SRS F-Area serves as one of the demonstration sites (U.S. DOE, 2010). The UQ toolset developed for ASCEM and applied in this study is named AGNI. Details on the sensitivity analysis method implemented in AGNI, and the approach followed for the UQ analyses are presented below.

6.1. UQ approach and methodology

In this study, AGNI was coupled with the TOUGHREACT code, using the PEST protocol (Doherty, 2008) as a pre- and post-processor for sampling the TOUGHREACT input parameter values and analyzing the simulation outputs. AGNI is now being coupled with a newly-developed ASCEM high performance computing simulator called AMANZI; the TOUGHREACT

Table 9
Physical and geochemical parameters considered in the uncertainty quantification (UQ) analysis.

Physical parameters						
Parameter	ID	Unit	Ref.	Lower	Upper	Unit
Permeability (**K**)	k_u	UUTRA	5×10^{-12}	2.51×10^{-12}	10^{-11}	[m^2]
	k_t	TCCZ	1.98×10^{-14}	2×10^{-15}	2×10^{-13}	[m^2]
	k_l	LUTRA	5×10^{-12}	2.5×10^{-12}	10^{-11}	[m^2]
Porosity (ϕ)	por_u	UUTRA	0.39	0.296	0.484	[−]
	por_t	TCCZ	0.39	0.296	0.484	[−]
	por_l	LUTRA	0.39	0.296	0.484	[−]
van Genuchten (α)	alpha_vg	UUTRA	4×10^{-4}	2.82×10^{-4}	5.62×10^{-4}	[kg^{-1} m^{-1} s^2]
van Genuchten (m)	m_vg	UUTRA	0.27	0.189	0.351	[−]
Groundwater recharge factor	f_rech		1	0.8	1.2	[−]
Basin seepage rate factor	f_basin		1	0.8	1.2	[−]
Geochemical parameters						
Parameter	ID	Unit	Ref.	Lower	Upper	Unit
Kaolinite specific surface area (diss./prec.)	k_kin_u	UUTRA	20.71	16.57	24.85	[m^2 g^{-1}]
Goethite specific surface area (diss./prec.)	g_kin_u	UUTRA	16.22	12.98	19.46	[m^2 g^{-1}]
Kaolinite specific surface area (sorption)	k_oh_u	UUTRA	20.71	16.57	24.85	[m^2 g^{-1}]
	k_oh_t	TCCZ	20.71	16.57	24.85	[m^2 g^{-1}]
	k_oh_l	LUTRA	20.71	16.57	24.85	[m^2 g^{-1}]
Goethite specific surface area (sorption)	g_oh_u	UUTRA	16.22	12.98	19.46	[m^2 g^{-1}]
	g_oh_t	TCCZ	16.22	12.98	19.46	[m^2 g^{-1}]
	g_oh_l	LUTRA	16.22	12.98	19.46	[m^2 g^{-1}]
Basin seepage chemical composition	H	pH	2.05	2.56	1.54	[−]
	NO3	Nitrates	10^{-2}	7.5×10^{-3}	1.25×10^{-2}	[mol kgw^{-1}]
	SO4	SO_4	4.8×10^{-5}	3.6×10^{-5}	6×10^{-5}	[mol kgw^{-1}]
	U	U(VI)	3.01×10^{-5}	2.26×10^{-5}	3.76×10^{-5}	[mol kgw^{-1}]
	Ca	Ca	10^{-5}	7.5×10^{-6}	1.25×10^{-5}	[mol kgw^{-1}]
	Na	Na	6.82×10^{-5}	5.1×10^{-5}	8.5×10^{-5}	[mol kgw^{-1}]

modeling and coupling to AGNI performed in this study are currently being used to benchmark AMANZI-based capabilities. AGNI includes several parameter sensitivity methods; the method implemented in this study is the Morris one-at-a-time (OAT) method (Morris, 1991), which is described further below.

Parameter sensitivity is commonly defined as a partial derivative of the change of the output variable caused by a unit change in each parameter from reference values (Cacuci, 2003). This is referred to as a local sensitivity approach, because it is dependent on a set of reference parameter values, unless the system is perfectly linear. Global sensitivity methods take multiple reference values of each parameter to explore the parameter space for identifying nonlinear/interaction effects, and also for honoring the impact of parameter uncertainty (Saltelli et al., 2005). The computational burden to cover permutations of the parameters is intensive, in general, especially when the number of parameters is large. The Morris OAT method is a type of global sensitivity method that is less computationally intensive than other methods, in large part because the number of required simulations is proportional to the number of input parameters (k) and not to the square of this value (k^2), as typically the case with other methods.

With the Morris OAT method, each parameter space (normalized as a uniform distribution in the [0,1] space) is partitioned into (p - 1) equally-sized sub-regions so that each parameter takes values from the set {0,1/(p - 1),2/(p - 1),…,1}. A fixed increment $\Delta = p/\{2(p - 1)\}$ is used to calculate the partial derivative for each parameter. From the reference point of each parameter randomly chosen from the set {0,1/(p - 1),2/(p - 1),…,1 - Δ}, the fixed increment is added to each parameter in a random order to compute the partial derivative of each parameter. The calculated partial derivative is called the "elementary effect" (EE) of each parameter. To complete one path to change each parameter (1 through k) once from one set of the reference values, the necessary number of model runs must be equal to $k + 1$. By having multiple paths (i.e., multiple permutations of reference parameter values and multiple orders to change each parameter), there are multiple EEs for each parameter. Taking the mean of EE can be regarded as a global sensitivity measure, since the mean EE represents the average effect of each parameter over the parameter space,

A number of 250 simulations were run with four partitions and ten paths for twenty-four flow and geochemical parameters ($p = 4$, $k = 24$, $r = 10$, where the total number of required runs is computed as $r * (k + 1) = 250$). Table 9 shows the ranges of uncertainty considered for the flow parameters (the permeability for each hydrogeological unit, the van Genuchten unsaturated zone parameters, the rate of natural recharge, and the seepage rate from the basin), and for the geochemical parameters (the specific mineral surface area for dissolution/precipitation and adsorption, as well as the chemical composition of the seepage solution). These uncertainty ranges were estimated on the basis of available historical data and previous parameter sensitivity analyses performed with modeling of the F-Area plume (Balakrishnan et al., 2003; Cook et al., 2002; Flach, 2010; Looney et al., 1987; Marine and Root, 1973).

6.2. UQ analysis results

To investigate the impact of variable flow and uncertain geochemical parameters on the acidic-U(VI) plume migration,

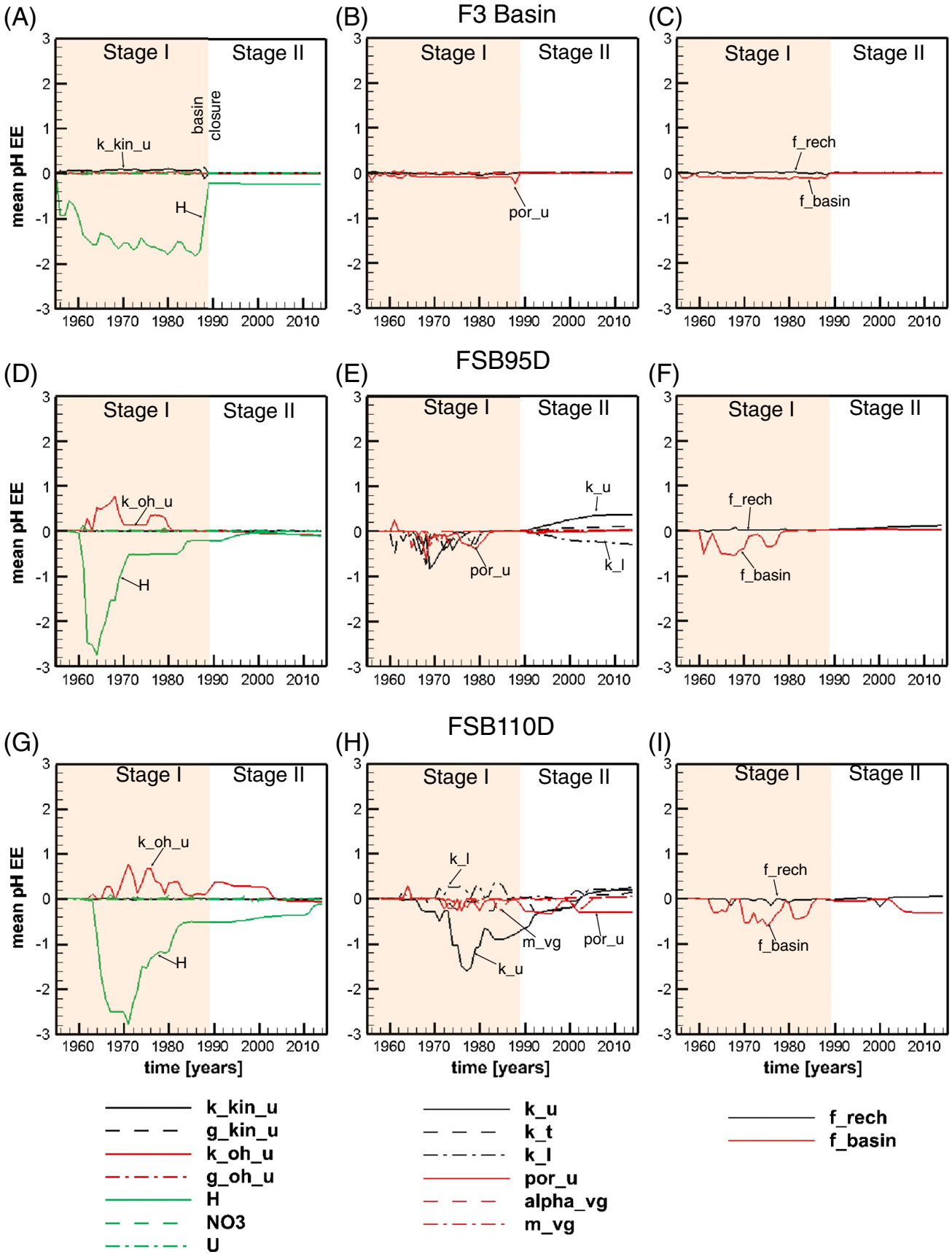

Fig. 6. Sensitivity of predicted pH values to model input parameters (see Table 9 for the curves legend explanation). Plots show the temporal evolution of the mean elementary sensitivity (EE) for pH at observation points: (A), (B) and (C) below the F-3 basin; (D), (E) and (F) at borehole FSB95D; and (G), (H) and (I) at borehole FSB110D.

we choose to examine predicted U(VI) concentrations and pH values at several modeled observation locations: (1) in the vadose zone immediately below the F-3 basin, (2) in the saturated zone of the UUTRA adjacent to the main basin (i.e., borehole FSB95), and (3) in the saturated zone of the UUTRA located ~300 m downgradient of the F3-basin (i.e., borehole

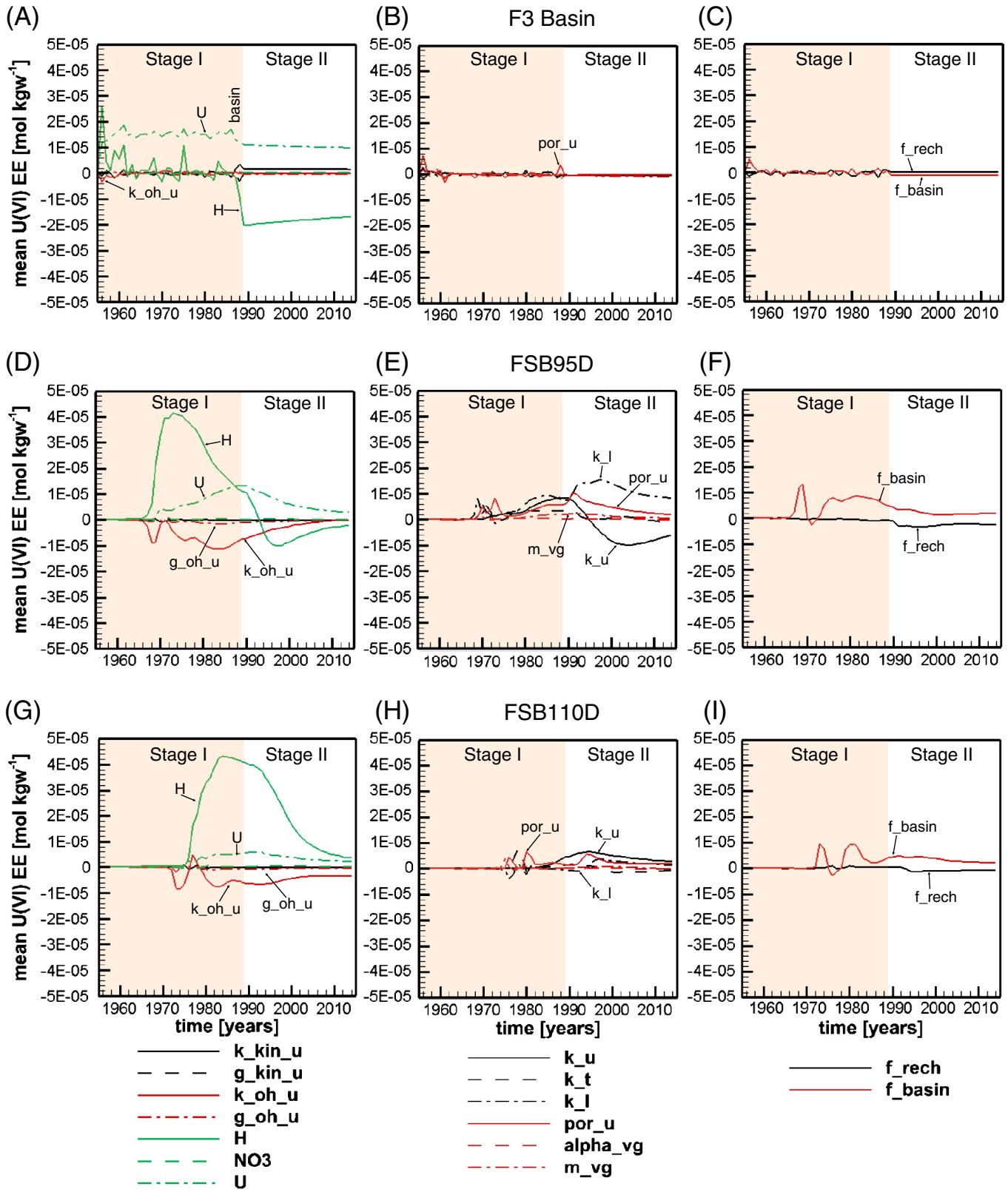

Fig. 7. Sensitivity of predicted U(VI) concentrations model input parameters (see Table 9 for the curves legend explanation). Plots show the temporal evolution of the mean elementary sensitivity (EE) for U(VI) at observation points: (A), (B) and (C) below the F-3 basin; (D), (E) and (F) at borehole FSB95D; and (G), (H) and (I) at borehole FSB110D.

FSB110, also located upstream from the pumping-treatment system cited in the "Site description" section). The temporal evolution of the mean EE for pH and U(VI) is shown in Figs. 6 and 7, respectively. The figures show that the predicted pH and U(VI) concentrations are sensitive to different flow and geochemical input parameters, and also this sensitivity evolves in space and time.

As would be expected, at all the observation locations, the predicted pH is mainly sensitive to the source pH (*H*) and the seepage rate (*f_basin*), emphasizing the importance of the source term during Stage I (Fig. 6D, F, G and I). In fact, pH sensitivity to the source pH (*H*) is around 20 times and 3 times larger than the second important parameter (i.e., kaolinite specific surface area of the UUTRA, *k_oh_u*). Results show a negative sensitivity for both these parameters, because increasing the H^+ loading lowers the pH of the groundwater. The sensitivity of predicted pH to these parameters progressively decreases at the end of Stage I to a more-or-less constant or zero value after closure, during Stage II. The sensitivity of predicted pH to flow parameters such as the permeability of the UUTRA and LUTRA (*k_u* and *k_l*, respectively) is larger away from the F-3 basin than near the basin (Fig. 6H). This indicates that differences in permeability have a progressively larger impact as the plume migrates through the vadose zone and farther downstream. During Stage I, the sensitivity of predicted pH to permeability of the UUTRA (*k_u*) is around 4 times larger than the permeability of the LUTRA (*k_l*). However, its sensitivity to permeability progressively decreases at the end of the Stage I and reverses during Stage II (e.g., see Fig. 6E). In this case, the increased permeability of the UUTRA enhances the mixing of the plume with the background groundwater after closure, and thus accelerates the pH rebound. The LUTRA permeability (*k_l*), on the other hand, has a significant impact on the pH evolution in the UUTRA near the basin, and to a lesser extent farther away. In the vicinity of the basin, an increasing the LUTRA permeability causes the groundwater to flow predominantly through this unit, which decreases the mixing in the UUTRA after the basin closure (resulting in lower predicted pH in this unit). However, the pH evolution farther downstream is dominated by the groundwater flow through the UUTRA. This implies that although geochemically the LUTRA is not as important as the UUTRA, its hydrological parameters influence the plume migration in the UUTRA near the basin.

The specific surface area of kaolinite for sorption (*k_oh_u*) exerts a control on the pH evolution both near and away from the F-3 basin (Fig. 6D and G), especially during Stage I. This is because an increase in the kaolinite specific surface area enhances the H^+ adsorption capacity of this mineral, and hence increases the pH buffering upon infiltration of acidic solutions. The sensitivity of predicted pH values to the surface area of kaolinite decreases to a constant then zero value during Stage II. This is because sorption sites become saturated from the huge influx of H^+ during Stage I for all cases of surface area considered, to the point when surface area is no longer relevant once all available sorption sites have filled up. It should be noted, however, that although the model sensitivity to sorption surface area becomes negligible during Stage II, H^+ desorption is still one of the dominant processes buffering pH to low values during Stage II, as discussed further below. The sensitivity of computed pH values to the UUTRA porosity (*por_u*, Fig. 6E and H) reflects the coupling effect with the specific surface area of kaolinite (*k_oh_u*), because the porosity directly affects the solid-to-water ratio and thus the sorption capacity of this mineral. The specific surface area of goethite (*g_oh_u*) has an effect similar to that of kaolinite, except that this mineral has a higher zero-point-of-charge than that of kaolinite. As a result, goethite becomes fully protonated at a pH higher (~5 to 6) than kaolinite (~3.5 to 4.5), thus has less impact on predicted pH values at low pH than kaolinite.

Predicted U(VI) concentrations in groundwater are sensitive mostly to the composition of the seepage solution, especially to its pH and U(VI) content, as would be expected (Fig. 7A and D). However, the sensitivity of predicted U(VI) concentrations to source pH (*H*) is around 3 to 10 times larger than source U(VI) content (*U*) progressively in those locations far away of the basin (Fig. 7D and G). Other parameters have negligible impact, at least during Stage I. The high sensitivity of predicted U(VI) concentrations to the source H^+ concentration at all locations (Fig. 7A, D and G) is evident because of the strong dependence of K_d values on pH, as discussed earlier (Fig. 5A and B). The nitrate concentrations (and other ions in the seepage solution) have a negligible effect on predicted U(VI) concentrations at all observed locations, reflecting weak competition with U(VI) for the adsorbed/exchanged sites onto kaolinite (Fig. 7A, D and G). Both near and far from the F-3 basin, the permeability of the UUTRA and LUTRA as well as the UUTRA porosity have a significant impact on predicted U(VI) concentrations, especially at the end of the Stage I and during Stage II (Fig. 7E and H). Near the basin, increasing the UUTRA permeability enhances transport/mixing, and thus yields a positive sensitivity of predicted U(VI) concentrations to permeability during Stage I (more U(VI) influx from the basin), but a negative sensitivity during Stage II (more attenuation from mixing with background water) (Fig. 7E). Away from the basin, predicted U(VI) concentrations display a positive sensitivity to the permeability of both the UUTRA and LUTRA (more U(VI) transport and delayed mixing with background water when the permeability is higher) (Fig. 7H). The UUTRA porosity (*por_u*) has an impact on U(VI) concentrations in the aquifers (most evident during Stage II), with increasing porosity reducing the available mineral surface area for adsorption (Fig. 7E and H). The vadose zone capillary properties (the van Genuchten parameter m in Eqs. (A4) and (A5); *m_vg* in Fig. 7E) play a role as well but to a lesser extent. Higher m values cause the plume in the vadose zone to drain more effectively into the groundwater, thus yield higher predicted U(VI) concentrations, especially during Stage II (Fig. 7E) once recharge from the basin has stopped.

The specific surface area of kaolinite (*k_oh_u*), and to a lesser extent of goethite (*g_oh_u*), exert an important control on the U(VI) concentrations both near and away from the basin (Fig. 7D and G). In fact, the sensitivity of predicted U(VI) concentrations to specific surface area of kaolinite (*k_oh_u*) is around 15 times larger than specific surface area of goethite (*g_oh_u*). Predicted U(VI) concentrations are particularly sensitive to these parameters as higher specific surface area tends to increase the plume retardation and adsorbed U(VI) concentrations. The sensitivity of predicted U(VI) concentrations to these parameters progressively decreases after Stage I as sorption sites become saturated, as discussed earlier for the case of pH.

For a better understanding of the system behavior, we also analyzed the breakthrough curves (BTCs) of pH and U(VI) concentrations near the basin (at FSB95D), output from

the simulations used in the UQ analyses (Fig. 8). The left column (Fig. 8A and C) shows the mean and 95% confidence interval of the breakthrough curves, and the right column (Fig. 8B and D) shows the dependence on the source pH. In Fig. 8B and D, the BTCs were divided into four groups (each separately colored in Fig. 8B and D) according to the source pH value assigned to the basin seepage. Note that these BTCs were based on systematic sampling of the parameter values for the sensitivity analysis, instead of random sampling commonly used in Monte-Carlo simulations. However, we consider that the variability of BTCs represents the uncertainty caused by the parameter uncertainty so that calculating the mean and confidence interval is meaningful.

In Fig. 8A, the variability of pH has different characteristics between the early time (pH decrease) and the later time (pH rebound). The variability of pH during the pH decrease is represented by different pH breakthrough times; the mean BTC does not represent any of the individual curves. The mean BTC indicates that the majority of pH breakthroughs happen between 1960 and 1970 except for the highest pH cases. On the other hand, the pH rebound happens at similar timing among different cases, but in different magnitudes. Therefore, at the beginning, the mean BTC indicates that the majority of U(VI) breakthroughs happens between 1980 and 2000.

In Fig. 8C, the timing of both concentration increase and decrease is widely distributed than pH, except for the highest source pH cases (Fig. 8D). The mean U concentration becomes the maximum at the end of Stage I. The confidence interval is large near the end of Stage I, and decreases during Stage II, which is different from pH. Overall, the confidence interval

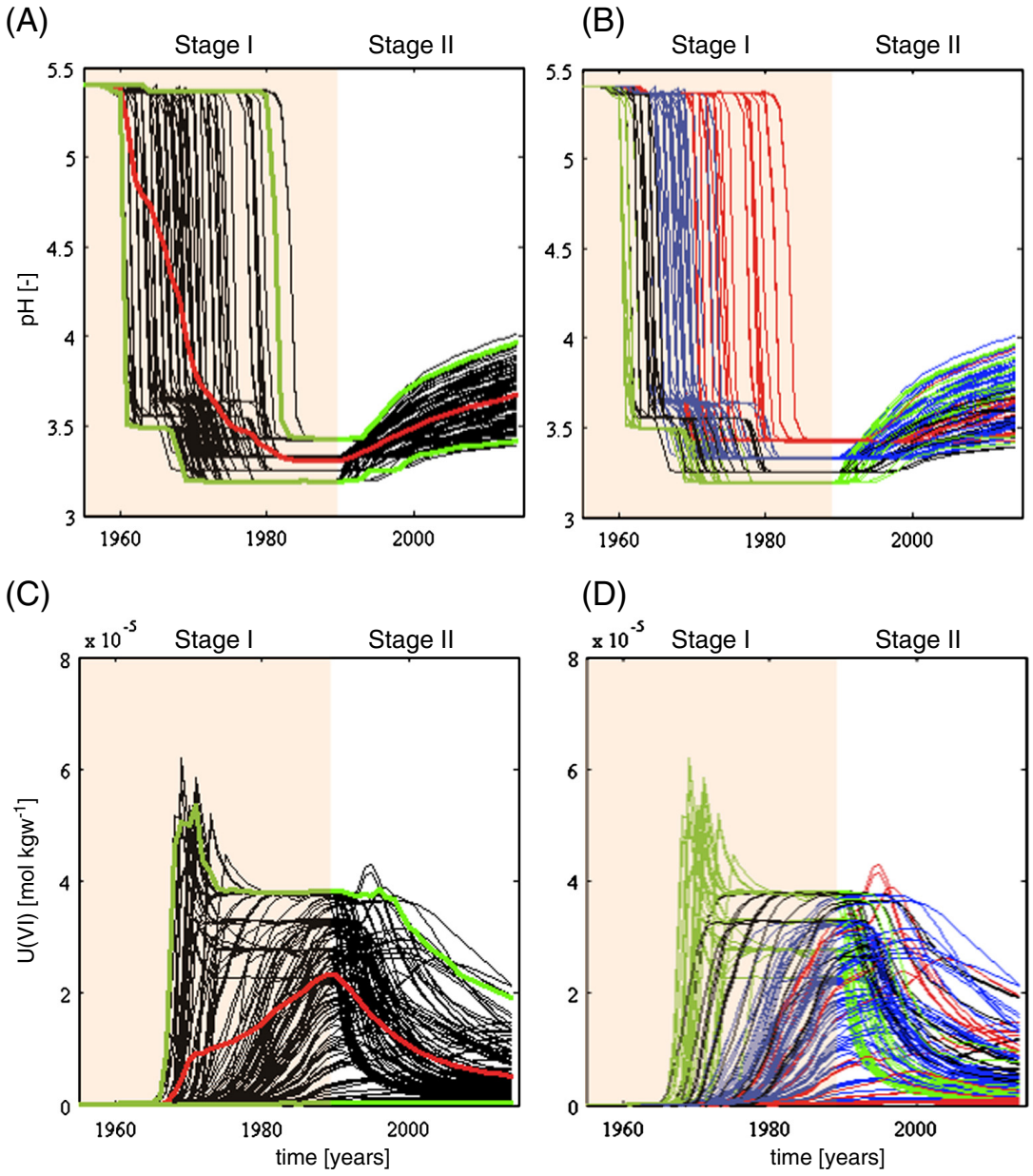

Fig. 8. Breakthrough curves of (A and B) pH, and (C and A) U(VI) at borehole FSB95D, output from the UQ model runs. The left column (A and C) shows the breakthrough curves with their mean and 95% confidence interval. The right column (D and B) shows the curves grouped into four sets (green, black, blue and red) corresponding to respectively higher source pH values (Table 9) (see text).

(hence uncertainty) of pH and U(VI) concentration has different characteristics.

The BTCs for pH show that the pH front is delayed when the source pH is higher (Fig. 8B), as would be expected. The forms of the pH BTCs are similar to those previously simulated with smaller-scale models of the F-Area Sassen et al. (2012). During Stage I, these curves display a typical H^+-titration step-like behavior, as the surfaces of first goethite, then kaolinite, then quartz get protonated, each time buffering pH to successively lower values in the order of decreasing PZC for these minerals (Fig. 8B). The source pH dictates the H^+ loading, thus dictates the time at which these surfaces get fully protonated. The strong pH buffering by surface protonation during Stage I dominates the effects of varying other parameters. As a result, varying parameters other than source pH during Stage I has comparatively less or no apparent effect. During Stage II, however, the pH rebound is strongly delayed by H^+ desorption and to a lesser extent by the precipitation of kaolinite and other Al phases. Because the H^+ loading onto sediments at the end of Stage I is huge in all cases of source pH considered, variations in source pH have much less direct effect on predicted pH values during Stage II than during Stage I, and varying other parameters has only a limited effect (i.e., in all cases the pH never rebounds back to background values).

The BTCs of U(VI) concentrations (Fig. 8D) show a behavior reverse that of the pH BTCs (Fig. 8B). The BTCs associated with the lowest source pH values present the shortest arrival times and highest concentrations at the plume front, because of increasing U(VI) mobility as pH decreases (Fig. 5A and B). The wave-shaped fronts are attributed to continuous U(VI) adsorption and subsequent desorption at the plume front during the loading stage (Stage I). After the basin closure during Stage II, the highest spread in U(VI) concentrations in the groundwater is predicted for the BTCs corresponding to the highest source pH range. This can be explained by the log-linear relationship between Kd values and pH (Fig. 5A), displaying an increasingly steeper sorption edge as pH increases within the pH range of interest here (~3 to 5.5).

7. Summary and conclusions

Numerical reactive transport (RT) simulations and sensitivity analyses were performed to assess hydraulic and geochemical processes controlling the migration and retardation of an acidic-U(VI) groundwater plume at the SRS F-Area. Seepage from the disposal of acidic solutions at this site for more than three decades has had a significant impact on both the vadose and saturated zones beneath the site. A nearly 1-km groundwater plume with historical pH values as low as ~3 and U(VI) concentrations as high as tens of micromolal has formed under the site, with the low pH driving U(VI) mobility. The adsorption of H^+ onto kaolinite and goethite and, to a lesser extent, dissolution and precipitation reactions involving Al minerals, have prevented the pH to rebound at this site since its closure more than 20 years ago. Simulated BTCs at several modeled locations (near and away from the main seepage basin) in the upper-most, water-table aquifer suggest that at least three concentration fronts have formed since the beginning of site operation. The first one consists of dissolved nitrates and ^3H, which are mostly unreactive species. The other two consecutive fronts consist of a low pH (high H^+) and high U(VI) fronts, also corresponding to gibbsite/kaolinite and kaolinite precipitation fronts, respectively. Kaolinite is predicted to immediately dissolve below the modeled basin, driven by the pH decrease, resulting in increased Al and Si concentrations in the pore water. Al is thus transported under acidic conditions first through the vadose zone, then into the saturated zone. Kaolinite is predicted to re-precipitate away from the basin. Gibbsite precipitates at the front of the plume where mixing with the background groundwater takes place. These model results are in agreement with, and complement, earlier smaller-scale simulations of acidic infiltration at the F-Area (Sassen et al., 2012; Spycher et al., 2011). Identified reactive processes through these simulations are also similar to processes observed and modeled by others for similar systems related to the attenuation of acidic plumes in groundwater systems (e.g., Gu et al., 2003; Zhu et al., 2001).

Sensitivity analyses were performed by integrating the TOUGHREACT code with the UQ platform AGNI developed through the ASCEM project. Results indicate that predicted pH and U(VI) concentrations in the unsaturated and saturated zones beneath the F-Area are sensitive to both physical (permeability, porosity; and the vadose zone retention curves parameters) and geochemical parameters (specific surface area of sorbing minerals and chemical composition of the seepage solution), and that the sensitivity of these predicted concentrations evolve in space and time. During the seepage stage, predicted pH and U(VI) concentrations are particularly sensitive to physical and geochemical parameters associated with the source term (i.e., seepage rate and chemical composition; specific surface area of kaolinite), while model results are more sensitive to hydrological parameters (permeability) after the basin closure (Figs. 6 and 7).

The pH and U(VI) concentrations in both the vadose and saturated zones are mainly sensitive to H^+ loading, because U(VI) is highly mobile under the acidic-pH range of groundwater at the F-Area (e.g., Dong et al., 2012). This contrasts with other studies at sites with more neutral groundwater, such as UQ efforts carried out at the Naturita site, Colorado, where predicted U(VI) concentrations were shown to be insensitive to source pH (Curtis et al., 2006). The predicted pH and U(VI) concentrations during Stage I are quite sensitive to the source pH. However, this sensitivity decreases during Stage II as mineral surface sites available for adsorption become saturated.

The specific surface area of kaolinite exerts a moderate control on the predicted pH and U(VI) concentrations in groundwater and its temporal influence increases downgradient of the modeled basin. This parameter also affects plume arrival times because it directly affects the total number of sorption sites available, and thus the time required to saturate these sorption sites. The sensitivity of predicted pH and U(VI) concentrations to porosity shows a behavior essentially similar to that of surface area (with an opposed sign), because porosity directly relates to the solid/water volume ratio and thus to the total area available for sorption. The permeability in the upper-most aquifer also exerts an important control on the plume migration and mixing with background groundwater at both the plume front and trailing edge. Other parameters such capillary properties of the vadose zone also have an effect although to a lesser extent.

The model and uncertainty quantification presented here are important to the closure strategy for the F-Area Seepage

Basins plume because of the insights they provide to the processes controlling pH rebound and how they affect estimates of timeframes for pH rebound. The current in situ remediation is a funnel and gate system with periodic pH adjustment within the gates designed to limit flux of contaminants to Fourmile Branch. The duration of its operation depends on pH rebound in the upgradient portion of the plume. Hence, understanding the rate of rebound and the processes controlling it informs future decisions on whether pH rebound in the upgradient portions needs engineered enhancement, and if so, how best to proceed.

Acknowledgments

This study was supported as part of the Subsurface Science Scientific Focus Area (SFA) funded by the U.S. Department of Energy, Office of Science, Office of Biological and Environmental Research to the Sustainable Systems SFA and by the ASCEM project, which is supported by U.S. Department of Energy Environmental Management, both under award number DE-AC02-05CH11231 to the LBNL. We sincerely thank Greg Flach (Savannah River National Laboratory) for the support in developing the site conceptual model and for providing the concentration data used in this study.

Appendix A

Flow Equations

In TOUGHREACT, the liquid mass balance under unsaturated conditions is formulated with the classical Richards equation as (Richards, 1931):

$$\frac{\delta\phi S_l\rho_l}{\delta t} = \nabla\cdot q_l + f_w\zeta \tag{A2}$$

where ϕ is the porosity [−], S_l is the pore water saturation [−], ρ_l is the pore water density [M L^{-3}], t is time [T], q_l is the water mass fluxes [M L^{-2} T^{-1}], f_w is a fluid source/sink term [M L^{-2} T^{-1}], and ζ is a constant that relates the surface area on the boundary to the volume of the porous medium [L^2 L^{-3}].

The water fluxes (q_l) induced by pressure gradients in Eq. (A2) are calculated based on Darcy's law:

$$q_l = \rho_l v_l = -\rho_l \frac{\mathbf{K}k_r}{\mu_l}(\nabla P_l + \rho_l g) \tag{A3}$$

where v_l is the modified Darcy flux [L T^{-1}], **K** is the permeability tensor [L^2], k_r is the relative permeability [−] as a function of pore water saturation (S_l), P_l is the pore water pressure [M L^{-1} T^{-2}], g is the gravity constant [L T^{-2}], and μ_l is the dynamic fluid viscosity [M L^{-1} T^{-1}]. Eqs. (A2) and (A3) are nonlinear, since the liquid pore saturation (S_l) and the relative permeability (k_r) are a function of the liquid pressure (P_l). Relationships given by Wösten and van Genuchten (1988) are normally used to describe these dependencies:

$$S_l = S_{rl} + \frac{1 + S_{rl}}{(1 + |\alpha P_c|^n)^m} \tag{A4}$$

$$k_r = S_{el}^p\left[1 - \left(1 - S_{el}^{1/m}\right)^m\right]^2 \tag{A5}$$

where p is a fitted parameter, P_c is the capillary pressure [M L^{-1} T^{-2}] defined as function of the atmospheric (P_{atm}) and liquid pressure as:

$$P_c = P_{atm} - P_l. \tag{A6}$$

The relative permeability (k_r) in Eq. (A3) is here conveniently expressed here as a function of liquid pore saturation (S_l), where S_{rl} defines the residual liquid pore saturation [−], α [M^{-1} L T^2], n [−], m [−] are the retention-curve parameters, p [−] is the Mualem (1976) parameter, and m is defined as:

$$m = 1 - \frac{1}{n}. \tag{A7}$$

S_{el} (Eq. (A5)) is the effective liquid pore saturation [-] and it is given by:

$$S_{el} = \frac{S_l - S_{rl}}{1 - S_{rl}} \tag{A8}$$

Reactive transport equations

Here, the Sequential Non-Iterative Approach (SNIA) is used for solving the coupled multicomponent reactive transport equations for N_c components (Xu et al., 2011):

$$\frac{\partial}{\partial t}\left(\phi S_l T_j^a\right) = \nabla\cdot v_l T_j^a - \nabla\cdot\phi S_l\tau_a D_a\nabla T_j^a + Q_j^a + f_j^a + f_j^\lambda, j = 1, N_c \tag{A9}$$

where v_l is the Darcy flux (Eq. (A3)), T_j^a is the total concentrations for j^{th} component in the aqueous phase [M L^{-3}], τ_a is the tortuosity for aqueous phase [−] computed here based on the relationships provided by Millington (1959), D_a is the aqueous diffusion tensor [L^2 T^{-1}], Q_j^a is the source/sink term for the j^{th} component due to the geochemical reactions [M L^{-3} T^{-1}], f_j^a is the source/sink term associated with boundary fluxes for the j^{th} component in the aqueous phase [M L^{-3} T^{-1}], and f_j^a accounts for the radioactive decay for the j^{th} component (in the present work only for the case of ^3H) as:

$$f_j^\lambda = -\lambda_j\phi S_l T_j^a \tag{A10}$$

where λ_j is the radioactive decay constant [T^{-1}] for the j^{th} component.

Permeability changes are considered coupled to chemical reactions (i.e., mineral dissolution/precipitation) through the porosity changes [$\mathbf{K}(\phi)$] using the Carman–Kozeny expression:

$$\mathbf{K}(\phi) = \frac{\phi^3}{(1-\phi)^2}\frac{(1-\phi_{ref})^2}{\phi^3}\mathbf{K_{ref}} \tag{A11}$$

where $\mathbf{K_{ref}}$ is the reference permeability tensor [L^2], and ϕ_{ref} is its associated reference porosity [−].

References

Arnold, T., Zorn, T., Zanker, H., Bernhard, G., Nitsche, H., 2001. Sorption behavior of U(VI) on phyllite: experiments and modeling. Journal of Contaminant Hydrology 47, 219–231.

Balakrishnan, S., Roy, A., Ierapetritou, M.G., Flach, G.P., Georgopoulos, P.G., 2003. Uncertainty reduction and characterization for complex environmental fate and transport models: an empirical Bayesian framework incorporating the stochastic response surface method. Water Resources Research 39 (12). http://dx.doi.org/10.1029/2002WR001810 (13 pp.).

Barnett, M.O., Jardine, P.M., Brooks, S.C., 2002. U(VI) adsorption to heterogeneous subsurface media: application of a surface complexation model. Environmental Science and Technology 36, 937–942.

Bethke, C.M., Brady, P.V., 2000. How the K_d approach undermines ground water cleanup. Ground Water 38, 435–443.

Boltz, D.R., 1997. Groundwater Model Recalibration and Remediation Well Network Design at the H-area Seepage Basins (U), Savannah River Site. U.S. Department of Energy Savannah River Site Technical Report WSRC-TR–97–121, Rev. 0..

Cacuci, D.G., 2003. Sensitivity and uncertainty analysis. Theory, vol. 1. Chapman and Hall/CRC Press, Boca Raton, FL.

Cahill, J., 1982. Hydrology of the low level radioactive solid waste burial site and vicinity near Barnwell, South Carolina. U.S. Geological Survey Open File Report 82-863..

Cook, J.R., Collard, L.B., Flach, G.P., Lee, P.L., 2002. Development of probabilistic uncertainty analysis methodology for SRS performance assessments maintenance plan activities, WSRC-TR-2002-00121. Westinghouse Savannah River Company LLC, Savannah River Site, Aiken, SC, USA.

Curtis, G.P., Davis, J.A., Naftz, D.L., 2006. Simulation of reactive transport of Uranium(VI) in groundwater with variable chemical conditions. Water Resources Research 42, W04404 (15 pp.).

Dai, M., Kelley, J.M., Buesseler, K.O., 2002. Sources and migration of plutonium in groundwater at the Savannah River Site. Environmental Science and Technology 36 (17), 3690–3699.

Davis, J., Meece, D., Kohler, M., Curtis, G., 2004. Approaches to surface complexation modeling of Uranium(VI) adsorption on aquifer sediments. Geochimica et Cosmochimica Acta 68 (18), 3621–3641.

Denehy, K., McMahon, P., 1985. Hydrologic and Micrometeorological Data for an Unsaturated Zone Flow Study at a Low Level Radioactive Waste Burial site, Barnwell, South Carolina. U.S. Geological Survey Open File Report OF85-476..

Denham, M.E., Vangelas, K.M., 2008. Biogeochemical gradients as a framework for understanding waste-site evolution. Remediation 19, 5–17.

Doherty, J., 2008. PEST: Model-Independent Parameter Estimation. Watermark Numerical Computing, Brisbane, Australia (http://pesthomepage.org/).

Dong, W., Brooks, S.C., 2006. Determination of the formation constants of ternary complexes of uranyl and carbonate with alkaline earth metals (Mg^{2+}, Ca^{2+}, Sr^{2+}, and Ba^{2+}) using anion exchange method. Environmental Science and Technology 40, 4689–4695.

Dong, W., Tokunaga, T., Davis, J., Wan, J., 2012. Uranium (VI) adsorption and surface complexation modeling under acidic conditions: background sediments from the F-Area Savannah River Site. Environmental Science and Technology 46, 1565–1571.

Fenimore, J.W., Horton, J., 1972. Rating History and Environmental Effects of Seepage Basins in the Chemical Separation Areas of the Savannah River Plant. USAEC report, DPST-72-548.USAEC, Washington, DC.

Flach, G.P., 2001. Analysis of Tritium and Strontium-90 Migration at the F- and H-Area Seepage Basins (U). WSRC-TR-2001-00xxx.Westinghouse Savannah River Company LLC, Savannah River Site, Aiken, SC 29808.

Flach, G.P., 2004. Groundwater flow model of the general separations area using Porflow (U). WSRC-TR-2004-00106.Westinghouse Savannah River Company LLC, Savannah River Site, Aiken, SC 29808.

Flach, G.P., 2010. Source term for ASCEM Phase I F-Seepage Basins Modeling Demonstration, SRNL-L6200-2010-00024. Savannah River National Laboratory, Aiken, SC, USA.

Flach, G.P., Harris, M.K., 1997. Integrated hydrogeological model of the general separations area. Groundwater Flow Model, Savannah River Site. U.S. Department of Energy, Savannah River Site: Technical Report WSRCTR-96-0399, volume 2.

Flach, G.P., Harris, M., Hlergesell, R., Smits, A., Hawkins, 1998. Hydrgeological and Groundwater Flow Model for C, K, L, and P Reactor Areas, Savannah River Site, Aiken, South Carolina (U). Westinghouse Savannah River Company (WSRC-TR-98–O0285. DOE, Contract No. DE-AC09–96SR18500).

Flach, G.P., Harris, M.K., Hiergesell, R.A., Smits, A.D., Hawkins, K.L., 1999. Regional groundwater flow model for C, K, L, and P reactor areas, Savannah River Site, Aiken, South Carolina (U), Savannah River Site. U.S. Department of Energy, Savannah River Site, Technical Report WSRCTR-99-00248, Rev. 0.

Flach, G.P., Crisman, S.A., Molz, F.J., 2004. Comparison of single-domain and dual-domain subsurface transport models. Ground Water 42, 815–828.

Gohn, G.S., 1988. Late Mesozoic and Early Cenozoic Geology of the Atlantic Costal Plains; North Carolina to Florida. In: Sheridan, R.E., Grow, J.A. (Eds.), The Geology of North America: Geol. Soc. Am., vol. 1–2, pp. 107–130.

Gu, B., Brooks, S.C., Roh, Y., Jardine, P.M., 2003. Geochemical reactions and dynamics during titration of a contaminated groundwater with high uranium, aluminum, and calcium. Geochimica et Cosmochimica Acta 67 (15), 2749–2761.

Guillaumont, R., Fanghänel, T., Neck, V., Fuger, J., Palmer, D.A., Grenthe, I., Rand, M., 2003. Update on the Chemical Thermodynamics of Uranium, Neptumium, Plutonium, Americium, and Technetium. Nuclear Energy Agency, Elsevier, Washington, DC.

Hammond, G.E., Lichtner, P.C., Rockhold, M.L., 2011. Stochastic simulation of uranium migration at the Hanford 300 area. Journal of Contaminant Hydrology 120 (21), 115–128.

Harris, M.K., Looney, B.B., Jackson, D.G., 2004. Geology and environmental remediation: Savannah River Site, South Carolina. Environmental Geosciences 11, 191–204.

Heidmann, I., Christl, I., Leu, L., Kretzschmar, R., 2005. Competitive sorption of protons and metal cations onto kaolinite: experiments and modeling. Journal of Colloid and Interface Science 282, 270–282.

Hubbard, J., Emslie, R., 1984. Water budget for the SRP burial ground area, Savannah River Site. U.S. Department of Energy, Savannah River Site, Technical Report DPST-83-742.

Jang, J., Dempsey, B., Burgos, W., 2007. A model-based evaluation of sorptive reactivities of hydrous ferric oxide and hematite for U(VI). Environmental Science and Technology 41, 4305–4310.

Jean, G.A., Yarus, J.M., Flach, G.P., Millings, M.R., Harris, M.K., Chambers, R.L., Syms, F.H., 2004. Three-dimensional geologic model of southeastern tertiary coastal-plain sediments, Savannah River Site, South Carolina: an applied geostatistical approach for environmental applications. Environmental Geosciences 11 (4), 205–220.

Kaplan, D., Bertsch, P., Adriano, D., 1995. Facilitated transport of contaminant metals through an acidified aquifer. Ground Water 33, 708–717.

Killian, T.H., Kolb, N.L., Corbo, P., Marine, I.W., 1986. Environmental information document, F-Area seepage basins. Report No. DPST 85-704.E.I. du Pont de Nemours & Co, Savannah River Laboratory, Aiken SC 29808.

Kohler, M., Curtis, G.P., Kent, D., Davis, J., 1996. Experimental investigation and modeling of uranium(VI) transport under variable chemical conditions. Water Resources Research 32 (12), 3539–3551.

Landry, C., Koretsky, C., Lund, T., Schaller, M., Das, S., 2009. Surface complexation modeling of Co(II) adsorption on mixtures of hydrous ferric oxide, quartz and kaolinite. Geochimica et Cosmochimica Acta 73, 3723–3737.

Lichtner, P.C., Felmy, A.R., 2003. Estimation of Hanford SX tank waste compositions from historically derived inventories. Computational Geosciences 29, 371–383.

Looney, B.B., Fenimore, J.W., Horton, J.H., 1972. Operating history and environmental effects of seepage basins in chemical separations areas of the Savannah River Plant. Report No. DPST-72-548.Westinghouse Savannah River Company, Savannah River Site, Aiken, South Carolina 29808.

Looney, B.B., Grant, M.W., King, C.M., 1987. Estimation of Geochemical Parameters for Assessing Subsurface Transport at the Savannah River plant, DPST-85-904. E.I. du Pont de Nemours and Company, Savanah River Laboratory, Aiken, SC.

Luo, W., Kelly, S., Kemner, K., Watson, D., Zhou, J., Jardine, P., Gu, B., 2009. Sequestering uranium and technetium through co-precipitation with aluminum in a contaminated acidic environment. Environmental Science and Technology 43, 7516–7522.

Mahoney, J.J., Cadle, S.A., Jakubowski, R.T., 2009. Uranyl adsorption onto hydrous ferric oxide-A re-evaluation for the diffuse layer model database. Environmental Science and Technology 43, 9260–9266.

Marine, I.W., Root, R.W., 1973. Summary of hydraulic conductivity tests in the SRP separation areas. Savannah River Laboratory Environmental Transport and Effects Research, Annual Report — FY 1975, DP-1412, Section 21.E.I. du Pont de Nemours and Company, Savannah River Laboratory, Aiken, SC.

Millings, M., Looney, B., Denham, M.E., 2012. Geochemical modeling of f area seepage basin composition and variability, SRNL-STI-2012-00269. Savannah River National Laboratory, Savannah River Nuclear Solutions, Aiken, SC 29808.

Millington, R.J., 1959. Gas diffusion in porous media. Science 130, 100–102.

Morris, M.D., 1991. Factorial sampling plans for preliminary computational experiments. Technometrics 33, 161–174.

Mualem, Y., 1976. A new model for predicting the hydraulic conductivity of unsaturated porous media. Water Resources Research 12, 512–522.

Newman, M., Elzerman, A., Looney, B., 1993. Facilitated transport of selected metals in aquifer material packed-columns. Journal of Contaminant Hydrology 14, 233–246.

Nordstrom, D., 1982. The effect of sulfate on aluminum concentrations in natural waters: some stability relations in the system Al_2O_3–SO_3–H_2O at 298 K. Geochimica et Cosmochimica Acta 46, 681–692.

Palandri, J., Kharaka, Y., 2004. A compilation of rate parameters of water–mineral interaction kinetics for application to geochemical modeling. U.S. Geological Survey. Open file report 2004-1068..

Parizek, R., Root Jr., R., 1986. Development of a ground-water velocity model for the radioactive waste management facility, Savannah River Plant, South Carolina. U.S. Department of Energy, Savannah River Site, Technical Report DPST-86-658.

Phifer, M., Millings, M., Flach, G., 2006. Hydraulic Property Data Package for the E-area and Z-Area Soils, Cementitious Materials, and Waste Zones. Washington Savannah River Company (WSRC-STI-2006-00198).

Pokrovskii, V.A., Helgeson, H.C., 1995. Thermodynamic properties of aqueous species and the solubilities of minerals at high pressures and temperatures: the system Al_2O_3–H_2O–NaCl. American Journal of Science 295, 1255–1342.

Read, D., Ross, D., Sims, R.J., 1998. The migration of uranium through Clashach Sandstone: the role of low molecular weight organics in enhancing radionuclide transport. Journal of Contaminant Hydrology 35, 235–248.

Richards, L.A., 1931. Capillary conduction of liquids through porous mediums. Physics 1 (5), 318–333.

Rimstidt, J.D., Barnes, H.L., 1980. The kinetics of silica–water reactions. Geochimica et Cosmochimica Acta 44 (11), 1683–1699.

Sadler, W.R., 1995. Groundwater Model Recalibration and Remediation Well Network Design at the F-area Seepage Basins (U), Savannah River Site. U.S. Department of Energy, Savannah River Site, Technical Report WSRC-RP-95-237.

Saltelli, A., Ratto, M., Tarantola, S., Campolongo, F., 2005. Sensitivity analysis for chemical models. Chemical Reviews 105, 2811–2828.

Sassen, D.S., Hubbard, S.S., Bea, S.A., Chen, J., Spycher, N., Denham, M.E., 2012. Reactive facies: an approach for parameterizing field-scale reactive transport models using geophysical methods. Water Resources Research 48, W10526. http://dx.doi.org/10.1029/2011WR011047.

Seaman, J.C., Looney, B.B., Harris, M.K., 2007. Research in support of remediation activities at the Savannah River Site. Vadose Zone Journal 6, 316–326.

Serkiz, S., Johnson, W., 1994. Uranium Geochemistry in Soil and Groundwater at the F and H Seepage Basins (EPD-SGS-94-307). Westinghouse Savannah River Co, Aiken, SC (United States) (ON: DE95002688; TRN: TRN: 94:010351).

Serkiz, S.M., Johnson, W.H., Wile, L.M.J., Clark, S.B., 2007. Environmental availability of uranium in an acidic plume at the Savannah River Site. Vadose Zone Journal 6, 354–362.

Sherman, D.M., Peacock, C.L., Hubbard, C.G., 2008. Surface complexation of U(VI) on goethite (α-FeOOH). Geochimica et Cosmochimica Acta 72, 298–310.

SNL (Sandia National Laboratories), 2007. Qualification of thermodynamic data for geochemical modeling of mineral–water interactions in dilute systems. In: Wolery, T.J., Jove Colon, C.F. (Eds.), Report ANL-WIS-GS-000003 REV 01. Sandia National Laboratories, Las Vegas, Nevada (ACC: DOC.20 070619.0007).

Sonnenthal, E., Spycher, N., 2000. Drift-scale Coupled Processes Model, Analysis and Model Report (AMR) N0120/U0110, Yucca Mountain Nuclear Waste Disposal Project. Lawrence Berkeley National Laboratory, Berkeley, California.

Spycher, N., Mukhopadhyay, S., Dassen, D., Murakami, H., Hubbard, S., Davis, J., Denham, M.E., 2011. On modeling H^+ and U transport behavior in an acidic plume. Goldschmidt Abstracts 2011. Mineralogical Magazine 75 (3), 1925.

Strom, R.N., Kaback, D.S., 1992. SRP baseline hydrogeologic investigation: aquifer characterization, groundwater geochemistry of the Savannah River site and vicinity. Report No. WSRC-RP-92-450 (DE93 003187). Environmental Sciences Section, Savannah River Laboratory, Westinghous Savannah River Company, Aiken, SC 29808.

Sverjensky, D.A., Sahai, N., 1996. Theoretical prediction of single-site surface-protonation equilibrium constants for oxides and silicates in water. Geochimica et Cosmochimica Acta 60, 3773–3797.

Tester, J.W., Worley, W.G., Robinson, B.A., Grigsby, C.O., Feerer, J.L., 1994. Correlating quartz dissolution kinetics in pure water from 25 °C to 625 °C. Geochimica et Cosmochimica Acta 58, 2407–2420.

Tokunaga, T.K., Wan, J., Denham, M.E., 2012. Estimates of vadose zone drainage from a capped seepage basin, F-Area, Savannah River Site. Vadose Zone Journal 11 (3).

U.S. DOE (Department of Energy), 2010. ASCEM phase I demonstration (Freshly M.D., Meza J., and Dixon P. Project Leads). Report Number ASCEM-SITE-102010-1. (December 16. URL: (http://esd.lbl.gov/files/research/projects/ascem/thrusts/application/Phase_1_Demo.pdf)).

U.S. EPA (Environmental Protection Agency), 1999. Understanding variation in partition coefficient, Kd, values. Report EPA 402-R-99-0044A, vol. 1 (Washington, DC).

Waite, T., Davis, J., Payne, T., Waychunas, G., Xu, N., 1994. Uranium(VI) adsorption to ferrihydrite: application of a surface complexation model. Geochimica et Cosmochimica Acta 58, 5465–5478.

Williamson, M., Meza, J., Moulton, D., Gorton, I., Freshley, M., Dixon, P., Seitz, R., Steefel, C., Finsterle, S., Hubbard, S., Zhu, M., Gerdes, K., Patterson, R., Collazo, Y.T., 2011. Advanced simulation capability for environmental management (ASCEM): an overview of initial results. Technology and Innovation 13, 175–199.

Wösten, J., van Genuchten, M., 1988. Using texture and other soil properties to predict the unsaturated soil hydraulic functions. Soil Science Society of America Journal 52, 1762–1770.

Xu, T., Spycher, N., Sonnenthal, E., Zhang, G., Zheng, L., Pruess, K., 2011. TOUGHREACT Version 2.0: a simulator for subsurface reactive transport under non-isothermal multiphase flow conditions. Computers & Geosciences 37, 763–774.

Yang, L., Steefel, C.I., 2008. Kaolinite dissolution and precipitation kinetics at 22 °C and pH 4. Geochimica et Cosmochimica Acta 72, 99–116.

Zhang, F., Parker, J.C., Brooks, S.C., Watson, D.B., Jardine, P.M., Gu, B., 2010. Prediction of uranium and technetium sorption during titration of contaminated acidic groundwater. Journal of Hazardous Materials 178, 42–48.

Zhang, F., Luo, W., Parker, J., Brooks, S., Watson, D., Jardine, P., Gu, B., 2011. Modeling uranium transport in acidic contaminated groundwater with base addition. Journal of Hazardous Materials 190, 863–868.

Zhu, C., Burden, D.S., 2001. Mineralogical compositions of aquifer matrix as necessary initial conditions in reactive contaminant transport models. Journal of Contaminant Hydrology 51, 145–161.

Zhu, C., Hu, F.Q., Burden, D.S., 2001. Multi-component reactive transport modeling of natural attenuation of an acid groundwater plume at a uranium mill tailings site. Journal of Contaminant Hydrology 52, 85–108.